

A Unified Implementation of Quasi-Monte Carlo Generators, Randomization Routines, and Fast Kernel Methods

ALEKSEI G SOROKIN, Illinois Institute of Technology, Department of Applied Mathematics, USA

Quasi-random sequences, also called low-discrepancy sequences, have been extensively used as efficient experimental designs across many scientific disciplines. This article provides a unified description and software API for methods pertaining to low-discrepancy point sets. These methods include low discrepancy point set generators, randomization techniques, and fast kernel methods. Specifically, we provide generators for lattices, digital nets, and Halton point sets. Supported randomization techniques include random permutations / shifts, linear matrix scrambling, and nested uniform scrambling. Routines for working with higher-order digital nets and scramblings are also detailed. For kernel methods, we provide implementations of special shift-invariant and digitally-shift invariant kernels along with fast Gram matrix operations facilitated by the bit-reversed FFT, the bit-reversed IFFT, and the FWHT. A new digitally-shift-invariant kernel of higher-order smoothness is also derived. We also describe methods to quickly update the matrix-vector product or linear system solution after doubling the number of points in a lattice or digital net in natural order.

CCS Concepts: • **Mathematics of computing** → **Statistical software**; *Mathematical software performance*; *Solvers*; Probabilistic algorithms.

Additional Key Words and Phrases: Low-discrepancy sequences, low-discrepancy point set randomizations, higher-order digital net scrambling, randomized Quasi-Monte Carlo, fast kernel methods, shift-invariant kernels, digitally-shift-invariant kernels

ACM Reference Format:

Aleksei G Sorokin. 2025. A Unified Implementation of Quasi-Monte Carlo Generators, Randomization Routines, and Fast Kernel Methods. *ACM Trans. Math. Softw.* 0, 0, Article 0 (2025), 25 pages. <https://doi.org/0.0>

1 Introduction

This article describes and implements a number of algorithms related to low-discrepancy point sets. These include implementations of

- low-discrepancy point set generators and randomizations,
- higher-order digital net generators and randomizations,
- shift-invariant and digitally-shift-invariant kernels of higher order smoothness,
- and fast transforms which enable fast Gram matrix operations when special kernels are paired with certain low-discrepancy point sets.

While these methods have been developed and often extensively studied throughout the literature, we found implementations to be scattered or even missing in some popular programming languages. Our main contribution is to provide a unified and accessible software for computations using low-discrepancy sequences in the QMCPy¹ Python package [Choi et al. 2022a,b]. We

¹<https://qmcpy.readthedocs.io>

Author's Contact Information: Aleksei G Sorokin, asorokin@hawk.iit.edu, Illinois Institute of Technology, Department of Applied Mathematics, Chicago, Illinois, USA.

Permission to make digital or hard copies of all or part of this work for personal or classroom use is granted without fee provided that copies are not made or distributed for profit or commercial advantage and that copies bear this notice and the full citation on the first page. Copyrights for components of this work owned by others than the author(s) must be honored. Abstracting with credit is permitted. To copy otherwise, or republish, to post on servers or to redistribute to lists, requires prior specific permission and/or a fee. Request permissions from permissions@acm.org.

© 2025 Copyright held by the owner/author(s). Publication rights licensed to ACM.

ACM 1557-7295/2025/0-ART0
<https://doi.org/0.0>

also integrate with the new LDData² repository which provides generating vectors for lattices and generating matrices for digital nets in standardized formats. This collection is, so far, mainly an aggregation of results from the Magic Point Shop³ [Kuo and Nuyens 2016a] and the websites of Frances Kuo on lattices⁴ [Cools et al. 2006; Nuyens and Cools 2006] and Sobol' points⁵ [Joe and Kuo 2003, 2008].

Below we summarize the novel components of our QMCPy software which we detail in this paper. Comparisons to existing implementations are also discussed. A more comprehensive review of Quasi-Monte Carlo software is given in [Choi et al. 2022b], along with more details on the QMCPy framework.

Lattice point sets We support generating points in linear, natural, or Gray code order and randomizing points with shifts modulo one. Other implementations of shifted lattices include those in MATLAB's GAIL⁶ (Guaranteed Automatic Integration Library) [Hickernell et al. 2018; Tong et al. 2022], the C++ LatNet Builder⁷ software [L'Ecuyer et al. 2021], and the multi-language MPS⁸ (Magic Point Shop) [Kuo and Nuyens 2016b]. LatNet Builder and MPS also provide search routines for finding good generating vectors which define lattice point sets.

Digital nets in base 2 We support generating digital nets in natural or Gray code order and randomizing with linear matrix scrambling (LMS) [Owen 2003], digital shifts, nested uniform scrambling (NUS) [Owen 1995], and permutation scrambling. To the best of our knowledge, we are also the only Python implementation to support digital interlacing for the creating of higher order digital nets and higher order scrambling with either LMS or NUS.

Early implementations of unrandomized digital sequences, including the Faure, Sobol' and Niederreiter-Xing constructions, can be found in [Bratley and Fox 2003; Bratley et al. 1992; Fox 1986; Pirsic 2002]. Considerations for implementing scrambles for digital sequences was discussed in [Hong and Hickernell 2003]. Recent digital net implementations supporting LMS and digital shifts include those in MPS, PyTorch [Paszke et al. 2019], SciPy [Virtanen et al. 2020], and MATLAB [Inc. 2022]. LatNet Builder provides robust support for all randomization routines and digital interlacing for higher order nets and scramblings. LatNet Builder and MPS also provide search routines for finding good generating matrices which define digital nets.

Halton point sets As with digital nets, we support randomizing Halton point sets with LMS, digital shifts, NUS, and permutation scrambles. The implementation of Halton point sets and randomizations have been treated in [Owen 2017; Wang and Hickernell 2000]. The QRNG⁹ (Quasi-Random Number Generators) R package [Hofert and Lemieux 2023] implements generalized digital nets which use optimized digital permutation scrambles; these are also supported in QMCPy. LatNet Builder also provides support for Halton points and their randomizations.

Kernel Methods and Fast Transforms We provide routines to evaluate special shift-invariant and digitally-shift-invariant kernels. This includes a new digitally-shift-invariant kernel of higher-order smoothness derived in this paper. These are not readily available elsewhere.

²<https://github.com/QMCSsoftware/LDData>

³<https://people.cs.kuleuven.be/~dirk.nuyens/qmc-generators/>

⁴<https://web.maths.unsw.edu.au/~fkuo/lattice/index.html>

⁵<https://web.maths.unsw.edu.au/~fkuo/sobol/index.html>

⁶http://gailgithub.github.io/GAIL_Dev/

⁷<https://github.com/umontreal-simul/latnetbuilder>

⁸<https://people.cs.kuleuven.be/~dirk.nuyens/qmc-generators/>

⁹<https://cran.r-project.org/web/packages/qrng/qrng.pdf>

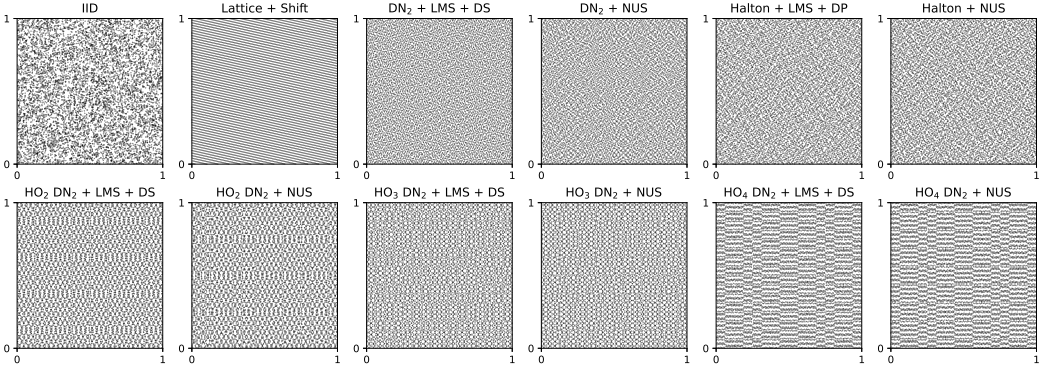


Fig. 1. An independent identically distributed (IID) point set and low-discrepancy (quasi-random) point sets of size $n = 2^{13} = 8192$. Notice the quasi-random points more evenly fill the space than IID points, which leads to faster convergence of Quasi-Monte Carlo methods compared to IID Monte Carlo methods. Randomized lattices, digital nets in base $b = 2$ (DN_2), and Halton points are shown. Randomizations include shifts, linear matrix scramblings (LMS), digital shifts (DS), and nested uniform scramblings (NUS). Digital interlacing of order α is used to create higher-order randomized digital nets (HO_α).

We also provide routines for fast matrix-vector multiplication and inversion of the nicely-structured Gram matrices produced when pairing these special kernels with certain low-discrepancy sequences. We also describe novel routines to efficiently update the matrix-vector products and linear system solves in the Gram matrix after doubling the number of lattice or digital net points. These fast operations are backed by implementations of the Fast Walsh Hadamard Transform (FWHT), the bit-reversed fast Fourier Transform (FFT), and the bit-reversed inverse FFT (IFFT). We are among the first to provide efficient and accessible Python interfaces to such fast kernel methods and the underlying fast transforms. GAIL has implemented fast Bayesian cubature routines utilizing this machinery.

These above routines are most commonly used in Quasi-Monte Carlo methods and for fast kernel methods, which we describe in the following subsections.

1.1 Quasi-Monte Carlo methods

Monte Carlo (MC) methods approximate a high dimensional integral over the unit cube by the sample average of function evaluations at certain sampling locations:

$$\mu := \int_{[0,1]^d} f(\mathbf{x}) d\mathbf{x} \approx \frac{1}{n} \sum_{i=0}^{n-1} f(\mathbf{x}_i) =: \hat{\mu}. \quad (1)$$

Here $f : [0,1]^d \rightarrow \mathbb{R}$ is a given integrand and $\{\mathbf{x}_i\}_{i=0}^{n-1} \in [0,1]^{n \times d}$ is a point set. The integral on the left hand side may be viewed as taking the expectation $\mathbb{E}[f(X)]$ where X is a standard uniform $X \sim \mathcal{U}[0,1]^d$. Classic MC methods choose the sampling locations to be independent and identically distributed (IID) d -dimensional standard uniforms $\mathbf{x}_0, \dots, \mathbf{x}_{n-1} \stackrel{\text{IID}}{\sim} \mathcal{U}[0,1]^d$. IID-MC methods for (1) have a root-mean-squared-error (RMSE) of $\mathcal{O}(n^{-1/2})$.

Quasi-Monte Carlo (QMC) methods [Dick et al. 2022; Dick and Pillichshammer 2010; Kroese et al. 2013; Lemieux 2009; Niederreiter 1992; Sloan and Joe 1994] replace IID point sets with low-discrepancy (LD) point sets which more evenly cover the unit cube $[0,1]^d$. For integrands with bounded variation, plugging LD point sets into $\hat{\mu}$ (1) yields a worst-case error rate of $\mathcal{O}(n^{-1+\delta})$ with $\delta > 0$

arbitrarily small. Some popular LD point sets are plotted in fig. 1 including lattices, digital nets (including higher-order versions), and Halton point sets.

Randomized Quasi-Monte Carlo (RQMC) uses randomized LD point sets to give improved convergence rates and enable practical error estimation. Specifically, if we again assume the integrand has bounded variation, then certain RQMC methods can achieve a RMSE of $\mathcal{O}(n^{-3/2+\delta})$. Moreover, let $\{\mathbf{x}_i^1\}_{i=0}^{n-1}, \dots, \{\mathbf{x}_i^R\}_{i=0}^{n-1}$ denote R IID randomizations of a low-discrepancy point set where typically R is small e.g. $R = 15$. Then the RQMC estimate

$$\widehat{\mu}_R = \frac{1}{R} \sum_{r=1}^R \widehat{\mu}^r \quad \text{where} \quad \widehat{\mu}^r = \frac{1}{n} \sum_{i=0}^{n-1} f(\mathbf{x}_i^r) \quad (2)$$

may be used to construct a practical (approximate) $100(1-\tau)\%$ confidence interval $\widehat{\mu}_R \pm t_{R-1, \tau/2} \widehat{\sigma}_R / \sqrt{R}$ for μ where $\widehat{\sigma}_R^2 = R^{-1}(R-1)^{-1} \sum_{r=1}^R (\widehat{\mu}^r - \widehat{\mu}_R)^2$ and $t_{R-1, \tau/2}$ is the $\tau/2$ quantile of a Student distribution with $R-1$ degrees of freedom. RQMC estimates are detailed in [Owen 2018, Chapter 17], and a recent comparison of RQMC confidence interval methods can be found in [L'Ecuyer et al. 2023]. QMC error estimation is treated more broadly in [Owen 2024], while [Clancy et al. 2014,?; Hickernell et al. 2017] detail additional considerations for adaptive QMC algorithms. For lattices, randomization is typically done using random shifts modulo 1. For digital nets, randomization is typically done using nested uniform scrambling (NUS) or the cheaper combination of linear matrix scrambling (LMS) with digital shifts / permutations [Owen 2003, 2017; Owen and Pan 2024].

Higher-order LD point sets were designed to yield faster convergence for integrands with additional smoothness. For integrands with square integrable mixed partial derivatives up to order $\alpha > 1$, plugging higher-order digital nets into $\widehat{\mu}(1)$ yields a worst-case error rate of $\mathcal{O}(n^{-\alpha+\delta})$ [Dick 2008, 2009a,b]. RQMC using scrambled digital nets (via either NUS or LMS with digital permutations) combined with digital interlacing has been shown to achieve an RMSE of order $\mathcal{O}(n^{-\alpha-1/2+\delta})$ [Dick 2011].

1.2 Kernel computations

Low-discrepancy (LD) point sets can also be used to accelerated many kernel computations. Let $\{\mathbf{x}_i\}_{i=0}^{n-1}$ be a point set, $K : [0, 1]^d \times [0, 1]^d \rightarrow \mathbb{R}$ be a symmetric positive definite (SPD) kernel, and $\mathbf{K} = (K(\mathbf{x}_i, \mathbf{x}_k))_{i,k=0}^{n-1}$ be the $n \times n$ SPD Gram matrix. Two motivating kernel computations are described below

Discrepancy Computation The error of the Monte Carlo approximation (1) can be bounded by the product two terms: a measure of variation of the function f and a measure of the discrepancy of the point set $\{\mathbf{x}_i\}_{i=1}^{n-1}$. The most well known bound of this type is the Koksma-Hlawka inequality [Dick et al. 2013; Hickernell 1998, 1999; Niederreiter 1992]. The discrepancy is frequently computed when designing and evaluating low-discrepancy point sets, see [Rusch et al. 2024] for a newer idea in this area where good point sets are generated using a neural networks trained with a discrepancy-based loss function.

Let us consider the more general setting of approximating the mean μ in (1) by a weighted cubature rule $\sum_{i=0}^{n-1} \omega_i f(\mathbf{x}_i)$. If f is assumed to lie in the RKHS H , the discrepancy in the error bound of such a cubature rule takes the form

$$\int \int K(\mathbf{u}, \mathbf{v}) d\mathbf{u} d\mathbf{v} - 2 \sum_{i=0}^{n-1} \omega_i \int K(\mathbf{u}, \mathbf{x}_i) d\mathbf{u} + \sum_{i,k=0}^{n-1} \omega_i \omega_k K(\mathbf{x}_i, \mathbf{x}_k)$$

following [Hickernell 1998]. Here the integrals are understood to be over the unit cube $[0, 1]^d$. Evaluating this discrepancy above requires computing $K\omega$ where $\omega = \{\omega_i\}_{i=0}^{n-1}$. Moreover, the discrepancy is minimized for a given point set by setting the weights to $\omega^* = K^{-1}\kappa$ where $\kappa_i = \int K(\mathbf{u}, \mathbf{x}_i) d\mathbf{u}$ for $0 \leq i < n$.

Kernel Interpolation Suppose we would like to approximate $f : [0, 1]^d \rightarrow \mathbb{R}$ given observations $\mathbf{y} = \{y_i\}_{i=0}^{n-1}$ of f at $\{\mathbf{x}_i\}_{i=0}^{n-1}$ satisfying $y_i = f(\mathbf{x}_i)$. Then a kernel interpolant approximates f by $\widehat{f} \in H$ where

$$\widehat{f}(\mathbf{x}) = \sum_{i=0}^{n-1} \omega_i K(\mathbf{x}, \mathbf{x}_i)$$

and $\omega = K^{-1}\mathbf{y}$. The above kernel interpolant may be reinterpreted as the posterior mean in Gaussian process regression, see [Williams and Rasmussen 2006]. Fitting a Gaussian process regression model often includes optimizing a kernel's hyperparameters, which also may be done by computing $K\omega$ and $K^{-1}\mathbf{y}$.

Underlying these problems, and many others, is the requirement to compute the matrix-vector product $K\mathbf{y}$ or solve the linear system $K\omega = \mathbf{y}$ for some length n vector \mathbf{y} . The standard cost of these computations are $O(n^2)$ and $O(n^3)$ respectively. One method to reduce these high costs is to induce structure into K . Structure-inducing methods pairing lattices and digital nets with special kernels were proposed in [Zeng et al. 2009] and shown to reduce the cost of both computations to $O(n \log n)$. Specifically, when a lattice point set $\{\mathbf{x}_i\}_{i=0}^{n-1}$ in linear order is paired with a shift-invariant kernel, K becomes circulant and computations can be performed using the fast Fourier transforms (FFT) and inverse FFT (IFFT). Similarly, when a base 2 digital net $\{\mathbf{x}_i\}_{i=0}^{n-1}$ is paired with a digitally-shift-invariant kernel, K becomes nested-block-Toeplitz and these computations can be performed using the Fast Walsh-Hadamard Transforms (FWHT) [Fino and Algazi 1976]. Such methods have recently been used to accelerate Bayesian cubature [Jagadeeswaran and Hickernell 2019, 2022; Rathinavel 2019] and solving PDEs with random coefficients [Kaarnioja et al. 2022, 2023].

We provide novel methods which exploit past solutions to $K\mathbf{y}$ or $K^{-1}\mathbf{y}$ when doubling the sample size from the LD sequence. This requires lattices are generated in natural order so we do not need to reorder outputs after doubling the sample size. We show that the same speedups can be achieved for lattices in natural order using bit-reversed FFT and bit-reversed IFFT algorithms. These bit-reversed algorithms simply skip the initial and final bit-reversal steps in the decimation-in-time FFT and IFFT respectively. We provide implementations of the bit-reversed FFT, bit-reversed IFFT, and FWHT.

Shift-invariant kernels of arbitrary smoothness are well known and can be computed based on the Bernoulli polynomials [Cools et al. 2021, 2020; Kaarnioja et al. 2022, 2023; Kuo et al. 2004; Sloan and Woźniakowski 2001]. Until now, digitally-shift-invariant kernels were only known for order 1 smoothness [Dick and Pillichshammer 2005]. We present higher-order digitally-shift-invariant kernels whose corresponding RKHSs contain functions of arbitrary smoothness. We derive closed forms of low order kernels (up to order 4 smoothness) in base $b = 2$, with the order 4 kernel not appearing elsewhere in the literature. These kernels are also of interest for computing the worst-case error of higher-order polynomial-lattice rules [Baldeaux et al. 2012], although we do not explore this connection here.

1.3 Outline

The remainder of this article is organized as follows. First, we describe our implementation in section 2. Section 3 discusses notation. Section 4 details rank 1 lattices, digital sequences, and Halton

sequences along with their randomization routines. Section 5 describes accelerated kernel computation with LD sequences, matching kernels, and fast transform algorithms. Section 6 provides numerical experiments. Finally, section 7 gives a brief conclusion and outlines directions for future work.

2 Implementation

We have implemented this work into QMCPy¹⁰ version 1.6, installable with `pip install -U qmcpy`. The architecture and philosophy underlying QMCPy are described in [Choi et al. 2022a,b]. To follow along with code snippets presented in this article, please import QMCPy and NumPy [Oliphant 2006] via

```
import qmcpy as qp
import numpy as np
```

These code snippets and code producing the plots in this article are available in notebook form¹¹.

Most of the QMCPy objects and methods presented here are wrappers around the lower level QMCToolsCL¹² package. The Python functions in QMCToolsCL often call lower level C implementations for improved performance. QMCToolsCL interfaces for other languages which support C extensions is a direction of future work.

3 Notation

Bold symbols denote vectors which are assumed to be column vectors e.g. $\mathbf{x} \in [0, 1]^d$. Capital letters in serif font denote matrices e.g. $K \in \mathbb{R}^{n \times n}$. Lower case letters in serif font denote digits in a base b expansion e.g. $i = \sum_{t=0}^{m-1} i_t b^t$ for $0 \leq i < 2^m$. This may be combined with bold notation when denoting the vector of base b digits e.g. $\mathbf{i} = (i_0, i_1, \dots, i_{m-1})^\top$. Modulo is always taken component-wise e.g. $\mathbf{x} \bmod 1 = (x_1 \bmod 1, \dots, x_d \bmod 1)^\top$. Permutations may be specified by vectors e.g. $\pi : \{0, 1, 2\} \rightarrow \{0, 1, 2\}$ with $\pi(0) = 2$, $\pi(1) = 0$, and $\pi(2) = 1$ may be denoted by $\pi = (2, 0, 1)$.

4 Low-discrepancy sequences and randomization routines

For a fixed base $b \in \mathbb{N}$, write $i \in \mathbb{N}_0$ as $i = \sum_{t=0}^{\infty} i_t b^t$ so i_t is the t^{th} digit in the base b expansion of i . We denote the vector of the first m base b digits of i by

$$D_m(i) = (i_0, i_1, \dots, i_{m-1})^\top.$$

For $\mathbf{i} = D_m(i)$ we use the notation

$$F_m(\mathbf{i}) = \sum_{t=1}^m i_{t-1} b^{-t}$$

to flip the digits of i about the decimal and convert back to a floating point number in $[0, 1)$. Finally, let

$$v(i) = \sum_{t=1}^{\infty} i_{t-1} b^{-t} \tag{3}$$

so that $v(i) = F_m(D_m(i))$ when $i < b^m$, which is always the case in this article. The Van der Corput sequence in base b is $(v(i))_{i \geq 0}$.

¹⁰<https://qmcpy.readthedocs.io>

¹¹https://github.com/QMCSsoftware/QMCSsoftware/blob/master/demos/ld_randomizations_and_higher_order_nets.ipynb

¹²<https://qmcssoftware.github.io/QMCToolsCL/>

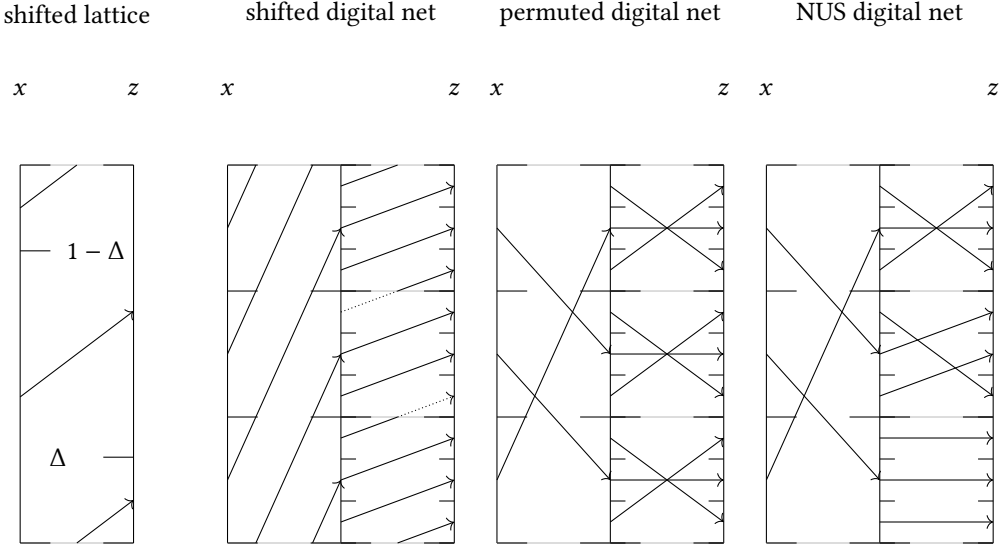


Fig. 2. Low-discrepancy randomization routines in dimension $d = 1$. Each vertical line is a unit interval with 0 at the bottom and 1 at the top. A given interval is partitioned at the horizontal ticks extending to the right, and then rearranged following the arrows to create the partition of the right interval as shown by the ticks extending to the left. For the shifted lattice and digitally shifted digital net, when the arrow hits a horizontal gray bar it is wrapped around to the next gray bar below. See for example the dotted line in the shifted digital net. The lattice shift is $\Delta = 0.227$. All digital nets use base $b = 3$ and $t_{\max} = 2$ digits of precision. The digital shift is $\Delta = (2, 1)^T$. Dropping the j subscript for dimension, the digital permutations in the third panel are $\pi_1 = (2, 0, 1)$ and $\pi_2 = (2, 1, 0)$. Notice π_1 is equivalent to a digital shift by 2, but π_2 cannot be written as a digital shift. The nested uniform scramble (NUS) has digital permutations $\pi = (2, 0, 1)$, $\pi_0 = (2, 1, 0)$, $\pi_1 = (0, 1, 2)$, and $\pi_2 = (1, 2, 0)$. Notice the permuted digital net in third panel has permutations depending only the current digit in the base b expansion. In contrast, the full NUS scrambling in the fourth panel has permutations which depend on all previous digits in the base b expansion.

4.1 Rank 1 lattices

Consider a fixed generating vector $g \in \mathbb{N}^d$ and fixed prime base b . Then we define the lattice sequence

$$z_i = v(i)g \pmod{1}, \quad i \geq 0.$$

If $n = b^m$ for some $m \in \mathbb{N}_0$, then the lattice point set $\{z_i\}_{i=0}^{n-1} \in [0, 1]^{n \times d}$ is equivalent to $\{i/ng \pmod{1}\}_{i=0}^{n-1}$ where we say the former is in natural order while the latter is in linear order.

Shifted lattice For a shift $\Delta \in [0, 1]^d$, we define the shifted point set

$$x_i = (z_i + \Delta) \pmod{1}$$

where z_i are lattice point set. The shift operation mod 1 is visualized in fig. 2. Randomized lattices use $\Delta \sim \mathcal{U}[0, 1]^d$. In the following code snippet we generate R independently shifted lattices with shifts $\Delta_1, \dots, \Delta_R \stackrel{\text{i.i.d.}}{\sim} \mathcal{U}[0, 1]^d$.

```
lattice = qp.Lattice(
    dimension = 52,
    randomize = "shift", # for unrandomized lattice set randomize = False
    replications = 16, # R
```

```

order = "natural", # also supports "linear" and "Gray" for Gray code
seed = None, # pass integer seed for reproducibility
generating_vector = "kuo.lattice-33002-1024-1048576.9125.txt")
x = lattice(2**16) # a numpy.ndarray with shape 16 x 65536 x 52

```

Here we have used a generating vector from [Cools et al. 2006] which is stored in a standardized format in the LDData repository. Other generating vectors from LDData may be used by passing in a file name from <https://github.com/QMCSsoftware/LDData/tree/main/lattice/> or by passing an explicit array.

4.2 Digital nets

Consider a fixed prime base b and generating matrices $C_1, \dots, C_d \in \{0, \dots, b-1\}^{t_{\max} \times m}$ where $m \in \mathbb{N}$ is fixed and b is a given prime base. One may relax the assumption that b is prime, but we do not consider that here or in the implementation. The first $n = b^m$ points of a digital sequence form a digital net $\{\mathbf{z}_i\}_{i=1}^{b^m-1} \in [0, 1)^{b^m \times d}$ in natural order. For $1 \leq j \leq d$ and $0 \leq i < b^m$ with digits $\mathbf{i} = D_m(i)$,

$$\mathbf{z}_{ij} = C_j \mathbf{i} \pmod{b} \quad \text{and} \quad z_{ij} = F_{t_{\max}}(\mathbf{z}_{ij})$$

where \mathbf{z}_{ij} is the base b expansion vector of z_{ij} .

Digitally shifted digital net Similar to lattices, one may apply a shift $\prime \in [0, 1)^{t_{\max} \times d}$ to the digital net to get a digitally-shifted digital net $\{\mathbf{x}_i\}_{i=0}^{b^m-1}$ where

$$\mathbf{x}_{ij} = F_{t_{\max}}((\mathbf{z}_{ij} + \Delta_j) \pmod{b})$$

and Δ_j is the j^{th} column of \prime . Randomly shifted digital nets use $\prime \stackrel{\text{iid}}{\sim} \mathcal{U}\{0, \dots, b-1\}^{t_{\max} \times d}$ i.e. each digit is chosen uniformly from $\{0, \dots, b-1\}$.

Digitally permuted digital net In what follows will denote permutations of $\{0, \dots, b-1\}$ by π . Suppose we are given a set of permutations

$$\prime = \{\pi_{j,t} : 1 \leq j \leq d, 0 \leq t < t_{\max}\}.$$

Then we may construct the digitally permuted digital net $\{\mathbf{x}_i\}_{i=1}^{b^m-1}$ where

$$\mathbf{x}_{ij} = F_{t_{\max}}((\pi_{j,0}(\mathbf{z}_{ij0}), \pi_{j,1}(\mathbf{z}_{ij1}), \dots, \pi_{j,t_{\max}-1}(\mathbf{z}_{ij(t_{\max}-1)})))^{\top}.$$

Randomly permuted digital nets use independent permutations chosen uniformly over all permutations of $\{0, \dots, b-1\}$.

Nested Uniform Scrambling (NUS) NUS is often called Owen scrambling for its conception in [Owen 1995]. As before, π values denote permutations of $\{0, \dots, b-1\}$. Now suppose we are given a set of permutations

$$\mathcal{P} = \{\pi_{j,v_1 \dots v_t} : 1 \leq j \leq d, 0 \leq t < t_{\max}, v_k \in \{0, \dots, b-1\} \text{ for } 0 \leq k \leq t\}.$$

Then a nested uniform scrambling of a digital net is $\{\mathbf{x}_i\}_{i=1}^{b^m-1}$ where

$$\mathbf{x}_{ij} = F_{t_{\max}}((\pi_j(\mathbf{z}_{ij0}), \pi_{j,z_{ij0}}(\mathbf{z}_{ij1}), \pi_{j,z_{ij0}z_{ij1}}(\mathbf{z}_{ij2}), \dots, \pi_{j,z_{ij0}z_{ij1} \dots z_{ij(t_{\max}-2)}}(\mathbf{z}_{ij(t_{\max}-1)})))^{\top}.$$

As the number of elements in \mathcal{P} is

$$|\mathcal{P}| = d(1 + b + b^2 + \dots + b^{t_{\max}-1}) = d \frac{b^{t_{\max}} - 1}{b - 1},$$

our implementation cannot afford to generate all permutations a priori. Instead, permutations are generated and stored only as needed. As with digitally-permuted digital nets, NUS uses independent uniform random permutations.

The randomization routines described above are visualized in fig. 2.

Linear matrix scrambling (LMS) is a computationally cheaper but less complete version of NUS which has proven sufficient for many practical problems. LMS uses scrambling matrices $S_1, \dots, S_d \in \{0, \dots, b\}^{t_{\max} \times t_{\max}}$ and sets the LMS generating matrices $\tilde{C}_1, \dots, \tilde{C}_d \in \{0, \dots, b\}^{t_{\max} \times m}$ so that

$$\tilde{C}_j = S_j C_j \pmod{b}$$

for $j = 1, \dots, d$. Following [Owen 2003], let us denote elements in $\{1, \dots, b\}$ by h and elements in $\{0, \dots, b\}$ by g . Then common structures for S_j include

$$\begin{pmatrix} h_{11} & 0 & 0 & 0 & \dots \\ g_{21} & h_{22} & 0 & 0 & \dots \\ g_{31} & g_{32} & h_{33} & 0 & \dots \\ g_{41} & g_{42} & g_{43} & h_{44} & \dots \\ \vdots & \vdots & \vdots & \vdots & \ddots \end{pmatrix}, \begin{pmatrix} h_1 & 0 & 0 & 0 & \dots \\ g_2 & h_1 & 0 & 0 & \dots \\ g_3 & g_2 & h_1 & 0 & \dots \\ g_4 & g_3 & g_2 & h_1 & \dots \\ \vdots & \vdots & \vdots & \vdots & \ddots \end{pmatrix}, \quad \text{and} \quad \begin{pmatrix} h_1 & 0 & 0 & 0 & \dots \\ h_1 & h_2 & 0 & 0 & \dots \\ h_1 & h_2 & h_3 & 0 & \dots \\ h_1 & h_2 & h_3 & h_4 & \dots \\ \vdots & \vdots & \vdots & \vdots & \ddots \end{pmatrix}$$

which corresponds to Matousek's linear scrambling [Matoušek 1998], Tezuka's i -binomial scrambling [Tezuka 2002], and Owen's striped LMS [Owen 2003] (not to be confused with NUS which is often called Owen scrambling). Random LMS chooses g and h values all independently and uniformly from $\{1, \dots, b\}$ and $\{0, \dots, b-1\}$ respectively. These scrambling are described in more detail and connected to NUS in [Owen 2003].

Digital interlacing enables the construction of higher-order digital nets. Denote the digitally interlaced version of $C_1, C_2, \dots \in \{0, \dots, b\}^{t_{\max} \times m}$ with interlacing factor $\alpha \in \mathbb{N}$ by $\tilde{C}_1, \tilde{C}_2, \dots \in \{0, \dots, b\}^{\alpha t_{\max} \times m}$. Then we have $\tilde{C}_{jtk} = C_{\tilde{j},k}$ where $\tilde{j} = \alpha(j-1) + (t \bmod \alpha) + 1$ and $\tilde{j} = \lfloor t/\alpha \rfloor$ for $j \geq 1$ and $0 \leq t < \alpha t_{\max}$ and $1 \leq k \leq m$. For example, with $m = 2$, $t_{\max} = 2$, and $\alpha = 2$ we have the following

$$\begin{aligned} C_1 &= \begin{pmatrix} c_{101} & c_{102} \\ c_{111} & c_{112} \end{pmatrix} & C_2 &= \begin{pmatrix} c_{201} & c_{202} \\ c_{211} & c_{212} \end{pmatrix} & C_3 &= \begin{pmatrix} c_{301} & c_{302} \\ c_{311} & c_{312} \end{pmatrix} & C_4 &= \begin{pmatrix} c_{401} & c_{402} \\ c_{411} & c_{412} \end{pmatrix} & \dots \\ \tilde{C}_1 &= \begin{pmatrix} c_{101} & c_{102} \\ c_{201} & c_{202} \\ c_{111} & c_{112} \\ c_{211} & c_{212} \end{pmatrix} & \tilde{C}_2 &= \begin{pmatrix} c_{301} & c_{302} \\ c_{401} & c_{402} \\ c_{311} & c_{312} \\ c_{411} & c_{412} \end{pmatrix} & & \dots \end{aligned}$$

Higher-order NUS requires NUS be applied to the digital net point sets generated by $C_1, \dots, C_{\alpha d}$ and then interlacing be performed to the digits $\{\mathbf{z}_{i1}\}_{i=0}^{b^m-1}, \dots, \{\mathbf{z}_{i,\alpha d}\}_{i=0}^{b^m-1}$ [Dick 2011]. For higher-order LMS, we apply LMS to the generating matrices $C_1, \dots, C_{\alpha d}$, then interlace them, then generate the digital net. As we shown in the numerical experiments in section 6, LMS is significantly faster than NUS (especially for higher-order nets) while still achieving higher-order rates of RMSE convergence.

A subtle difference between the above presentation and practical implementation is that t_{\max} may change with randomization in practice. For example, suppose we are given generating matrices $C_1, \dots, C_d \in \{0, \dots, b-1\}^{32 \times 32}$ but would like the shifted digital net to have 64 digits of precision. Then we should generate $\Delta \in \{0, \dots, b-1\}^{t_{\max} \times d}$ with $t_{\max} = 64$ and treat C_j as $t_{\max} \times t_{\max}$ matrices with appropriate rows and columns zeroed out.

Gray code ordering of digital nets enables computing the next point \mathbf{x}_{i+1} from \mathbf{x}_i by only adding a single column from each generating matrix rather. Specifically, the q^{th} column of each generating matrix gets digitally added to the previous point where $q-1$ is the index of the only digit to be changed in Gray code ordering. Gray code orderings for $b = 2$ and $b = 3$ are shown in table 1.

i	i_2	Gray code i_2	i_3	Gray code i_3
0	0000 ₂	0000 ₂	00 ₃	00 ₃
1	0001 ₂	0001 ₂	01 ₃	01 ₃
2	0010 ₂	0011 ₂	02 ₃	02 ₃
3	0011 ₂	0010 ₂	10 ₃	12 ₃
4	0100 ₂	0110 ₂	11 ₃	11 ₃
5	0101 ₂	0111 ₂	12 ₃	10 ₃
6	0110 ₂	0101 ₂	20 ₃	20 ₃
7	0111 ₂	0100 ₂	21 ₃	21 ₃
8	1000 ₂	1000 ₂	22 ₃	22 ₃

Table 1. Gray code order for bases $b = 2$ and $b = 3$. In Gray code order only one digit is incremented or decremented by 1 (modulo b) when i is incremented by 1.

The following code generates a base 2 digital net with R independent LMS, R independent digital shifts, and $\alpha = 2$ interlacing.

```

dnb2 = qp.DigitalNetB2(
    dimension = 52,
    randomize = "LMS_DS", # Matousek's LMS with a digital shift
    # options are [LMS_DS, NUS, DS, LMS, False]
    t_lms = 64, # number of LMS bits i.e. number of rows in S_j
    alpha = 2, # interlacing factor for higher order digital nets
    replications = 15, # R
    graycode = False, # use natural order instead of Gray code order
    seed = None, # pass integer seed for reproducibility
    generating_matrices = "LDData:mps.sobol-Cs.txt")
x = dnb2(2**16) # a numpy.ndarray with shape 15 x 65536 x 52

```

Here we have used a set of Sobol' generating matrices from Joe and Kuo¹³ [Joe and Kuo 2008] which are stored in a standardized format in the LDData repository. Other generating matrices from LDData may be used by passing in a file name from <https://github.com/QMCSsoftware/LDData/blob/main/dnet/> or by passing an explicit array.

4.3 Halton sequences

The digital sequences described in the previous section used a fix prime base b . One may allow each dimension $j \in \{1, \dots, d\}$ to have its own prime base b_j . The most popular of such constructions is the Halton sequence which sets b_j to the j^{th} prime, sets C_j to the identity matrix, and sets $t_{\max} = m$. This enables the simplified construction of Halton points $\{\mathbf{x}_i\}_{i=0}^{n-1}$ via

$$\mathbf{x}_i = (v_{b_1}(i), \dots, v_{b_d}(i))^{\top}$$

where we have added a subscript to v in (3) to denote the base dependence.

Almost all the methods described for digital sequences are immediately applicable to Halton sequences after accounting for the differing bases across dimensions. However, digital interlacing is not generally applicable when the bases differ. Halton with random starting points has also been explored in [Wang and Hickernell 2000], although we do not consider this here. The following code generates a Halton point set with R independent LMS and R independent digital permutations.

¹³the "new-joe-kuo-6.21201" direction numbers from <https://web.maths.unsw.edu.au/~fkuo/sobol/index.html>

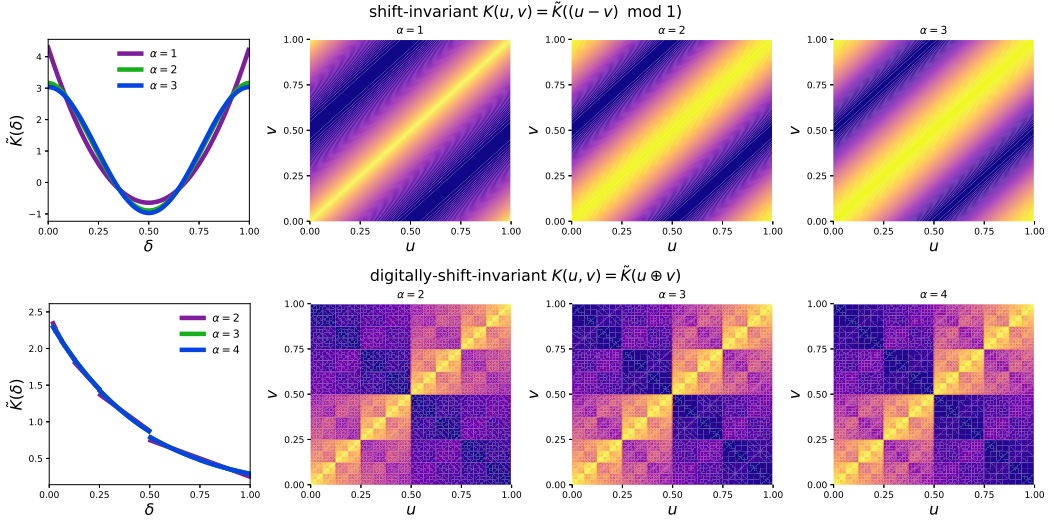


Fig. 3. Shift-invariant kernels (top row) and digitally-shift-invariant kernels (bottom row). Here α denotes the smoothness of the kernel. The $\alpha = 3$ and $\alpha = 4$ digitally-shift-invariant kernels are nearly indistinguishable. Shift-invariant kernels are described in section 5.1 while digitally-shift-invariant kernels are described in section 5.2.

```

halton = qp.Halton(
    dimension = 52,
    randomize = "LMS_PERM", # Matousek's LMS with a digital permutation
    # options are [LMS_PERM, LMS_DS, LMS, PERM, DS, NUS, QRNG, FALSE]
    t_lms = 64, # number of LMS digits i.e. number of rows in S_j
    replications = 15, # R
    seed = None) # pass integer seed for reproducibility
x = halton(2**10) # a numpy.ndarray with shape 15 x 1024 x 52

```

The QRNG randomization follows the QRNG software package [Hofert and Lemieux 2023] in generating a generalized Halton point set [Faure and Lemieux 2009] using a deterministic set of permutation scrambles and random digital shifts.

5 Fast transforms and kernel computations

Recall from the introduction that we would like to compute the matrix-vector product $\mathbf{K}\mathbf{y}$ and solve the linear system $\mathbf{K}^{-1}\mathbf{y}$ where \mathbf{y} is some known length n vector and $\mathbf{K} = \{K(\mathbf{x}_i, \mathbf{x}_k)\}_{i,k=0}^{n-1}$ is a $n \times n$ symmetric positive definite (SPD) Gram matrix based on an SPD kernel K and point set $\{\mathbf{x}_i\}_{i=0}^{n-1}$. We may reduce the standard $\mathcal{O}(n^2)$ and $\mathcal{O}(n^3)$ costs of solving these respective problems to both be $\mathcal{O}(n \log n)$ by inducing structure into \mathbf{K} using special point set-kernel pairings. Specifically, pairing lattice points with a shift invariance kernel yields a circulant Gram matrix \mathbf{K} for which computations can be done quickly using the bit-reversed fast Fourier transform (FFT) and bit-reversed inverse FFT (IFFT). Similarly, pairing a digital net with digitally-shift-invariant kernel yields a nested block Toeplitz matrix for which computations can be done quickly using the fast Walsh Hadamard Transform (FWHT). Shift-invariant and digitally-shift-invariant kernels are shown in fig. 3. The reduced costs achieved by inducing these structures are summarized in table 2.

$\{\mathbf{x}_i\}_{i=0}^{n-1}$	K structure	K storage	K decomposition	$\mathbf{K}\mathbf{y}$ cost	$\mathbf{K}^{-1}\mathbf{y}$ cost	methods
general	SPD	$\mathcal{O}(n^2)$	$\mathcal{O}(n^3)$	$\mathcal{O}(n^2)$	$\mathcal{O}(n^2)$	standard
lattice	SPD SI	$\mathcal{O}(n)$	$\mathcal{O}(n \log n)$	$\mathcal{O}(n \log n)$	$\mathcal{O}(n \log n)$	FFT-based
digital net	SPD DSI	$\mathcal{O}(n \log n)$	$\mathcal{O}(n)$	$\mathcal{O}(n \log n)$	$\mathcal{O}(n \log n)$	FWHT-based

Table 2. Comparison of storage and cost requirements for kernel methods. Decomposition of the symmetric positive definite (SPD) Gram matrix \mathbf{K} is the cost of computing the eigendecomposition or Cholesky factorization. The costs of matrix-vector multiplication and solving a linear system are the costs after performing the decomposition. Both storage and kernel computation costs are greatly reduced by pairing certain low-discrepancy point sets with special shift-invariant (SI) or digitally-shift-invariant (DSI) kernels.

The following code can be used to construct a Gram matrix with a lattice point set and shift-invariant kernel. The Gram matrix is then used to perform matrix-vector multiplication and solve a linear system. Analogous code using `qp.DigitalNetB2`, `qp.KernelDigShiftInvar`, and `qp.FastGramMatrix` is also supported.

```
d = 5 # dimension
n = 2**20 # 2^20 points
dd_obj = qp.Lattice(dimension=d, seed=7)
# qp.Lattice defaults to natural ordering with a single random shift
kernel_obj = qp.KernelShiftInvar( # matching kernel
    dimension = d,
    lengthscales = 0.1*np.ones(d, dtype=float), # product weights
    alpha = 4*np.ones(d, dtype=int)) # smoothness parameters
K = qp.FastGramMatrixLattice( # n x n Gram matrix
    kernel_obj = kernel_obj,
    dd_obj = dd_obj,
    n1 = n,
    n2 = n)
y = np.random.rand(n) # get a random length n vector
a = K@y # compute the matrix-vector product a=Ky at O(n log n) cost
b = K.solve(y) # solve linear system Kb=y for b at O(n log n) cost
```

Schematics of the bit-reversed FFT and FWHT underlying these fast computations are shown in fig. 4. The one-dimensional bit-reversed FFT, one-dimensional bit-reversed IFFT, and one-dimensional FWHT are implemented into the QMCPy functions `qp.fftbr`, `qp.ifftbr`, and `qp.fwht` respectively. These fast transforms act along the last dimension which is required to have length 2^m for some $m \geq 0$. The following subsections detail the matching point set-kernel pairings and provide methods to quickly update the Gram matrix product or linear system solution after doubling the point size.

5.1 Shift invariant kernels, lattices, and the bit-reversed FFT/IFFT

A kernel is said to be shift-invariant when $K(\mathbf{u}, \mathbf{v}) = \tilde{K}((\mathbf{u} - \mathbf{v}) \bmod 1)$ for some \tilde{K} i.e. the kernel is only a function of the component-wise difference between inputs modulo 1. One set of shift-invariant kernels take the form

$$K(\mathbf{u}, \mathbf{v}) = \sum_{\mathbf{u} \subseteq \mathcal{D}} \gamma_{\mathbf{u}} \prod_{j \in \mathbf{u}} \eta_{\alpha_j}((u_j - v_j) \bmod 1) \quad (4)$$

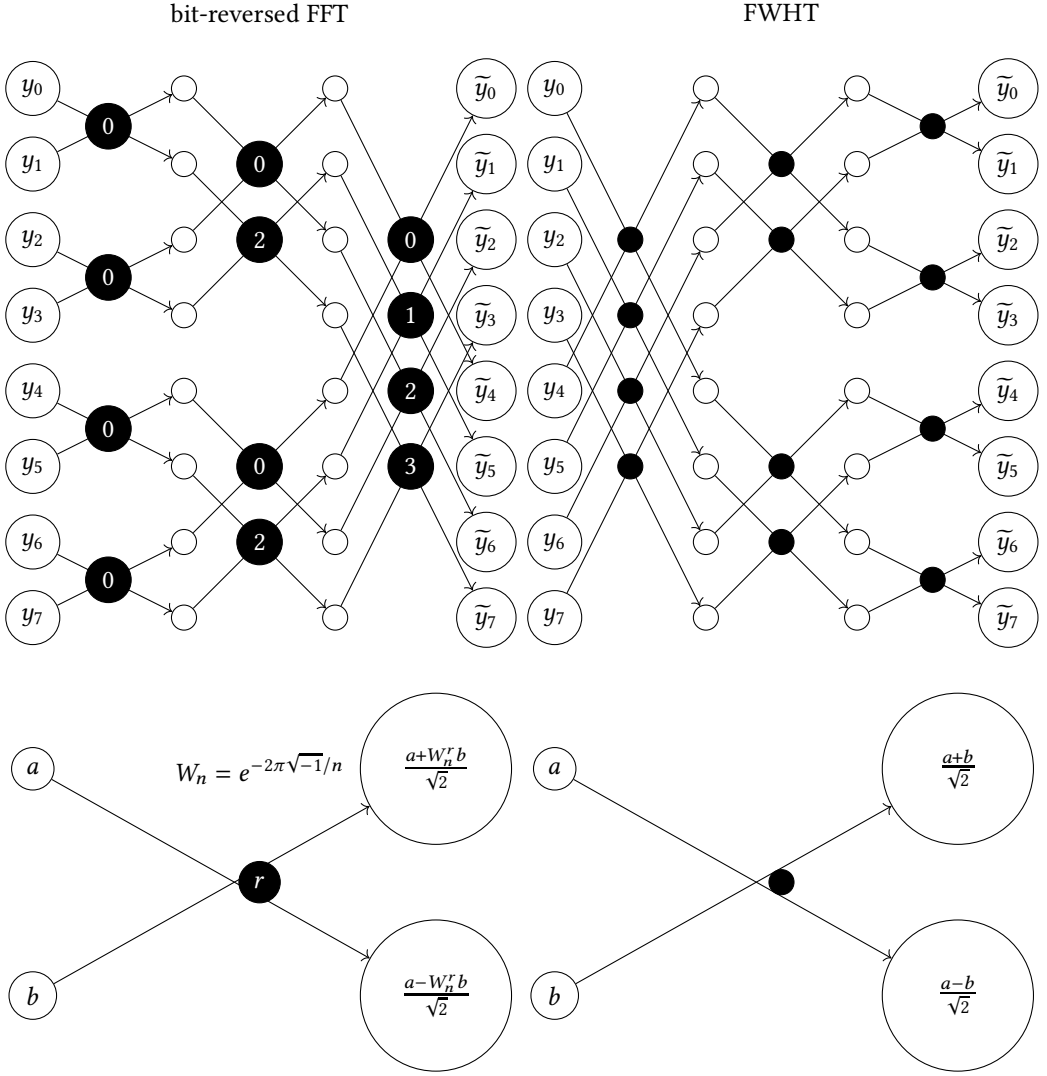


Fig. 4. Bit-reversed FFT and FWHT schemes. The bit-reversed FFT is performed via a decimation in time algorithm without the initial reordering of inputs. The bit-reversed IFFT may be performed by propagating $\{\tilde{y}_i\}_{i=0}^{2^m-1}$ to $\{y_i\}_{i=0}^{2^m-1}$ in the other direction through the bit-reversed FFT algorithm.

where

$$\eta_\alpha(\delta) = \frac{(2\pi)^{2\alpha}}{(-1)^{\alpha+1}(2\alpha)!} B_{2\alpha}(\delta)$$

with $\alpha \in \mathbb{N}^d$, $\mathcal{D} = \{1, \dots, d\}$, weights $\{\gamma_u\}_{u \in \mathcal{D}}$, and B_ℓ denoting the Bernoulli polynomial of degree ℓ . The corresponding reproducing kernel Hilbert space (RKHS) H is a weighted periodic unanchored Sobolev space of smoothness $\alpha \in \mathbb{N}^d$ with norm

$$\|f\|_H^2 := \sum_{u \in \mathcal{D}} \frac{1}{(2\pi)^{2|u|} \gamma_u} \int_{[0,1]^{|u|}} \left| \int_{[0,1]^{s-|u|}} \left(\prod_{j \in u} \frac{\partial^{\alpha_j}}{\partial y_j^{\alpha_j}} \right) f(\mathbf{y}) d\mathbf{y}_{-u} \right|^2 d\mathbf{y}_u,$$

where $f : [0, 1]^d \rightarrow \mathbb{R}$, $\mathbf{y}_u = (\mathbf{y}_j)_{j \in u}$, $\mathbf{y}_{-u} := (\mathbf{y}_j)_{j \in \mathcal{D} \setminus u}$, and $|u|$ is the cardinality of u . The space H is a special case of the weighted Korobov space which has real smoothness parameter α characterizing the rate of decay of Fourier coefficients, see e.g. [Cools et al. 2021, 2020; Kaarnioja et al. 2022, 2023; Kuo et al. 2004; Sloan and Woźniakowski 2001].

The kernel (4) is the sum over 2^d terms and thus becomes impractical to compute for large d . A simplified space assumes γ_u are product weights which take the form $\gamma_u = \prod_{j \in u} \gamma_j$ for some $\{\gamma_j\}_{j=1}^d$. The kernel with product weights takes the simplified form

$$K(\mathbf{u}, \mathbf{v}) = \prod_{j=1}^d \left(1 + \gamma_j \eta_{\alpha_j}((u_j - v_j) \bmod 1) \right). \quad (5)$$

Figure 3 shows one dimensional shift-invariant kernels with unit weight and varying smoothness. See [Kaarnioja et al. 2023] for a review of lattice-based kernel interpolation in such weighted spaces along with the development of serendipitous weights, which are a special form of high-performance product weights.

Suppose $n = 2^m$ for some $m \in \mathbb{N}_0$ and let $\{\mathbf{x}_i\}_{i=0}^{b^m-1}$ be a shifted lattice with shift $\Delta \in [0, 1)^d$ generated in linear order. For $0 \leq i, k < n$

$$K(\mathbf{x}_i, \mathbf{x}_k) = K\left(\frac{(i-k)\mathbf{g}}{n}, \mathbf{0}\right),$$

so the Gram matrix K is circulant. Let $R_m(i)$ flip the first m bits of $0 \leq i < 2^m$ in base $b = 2$ so that if $i = \sum_{t=0}^{m-1} i_t 2^t$ then $R(i) = \sum_{t=0}^{m-1} i_{m-t-1} 2^t$. The first step in the FFT with decimation-in-time is to reorder the inputs $\{y_i\}_{i=0}^{2^m-1}$ into bit reversed order $\{y_{R(i)}\}_{i=0}^{2^m-1}$. The last step in computing the IFFT is to reorder the outputs $\{y_{R(i)}\}_{i=0}^{2^m-1}$ into bit reversed order $\{y_i\}_{i=0}^{2^m-1}$. Therefore, one should generate lattice points in natural order and skip the first step of the FFT and last step of the inverse FFT.

The Fourier matrix is $\overline{F^{(m)}} = \{W_m^{ij}\}_{i,j=0}^{2^m-1}$ where $W_m = \exp(-2\pi\sqrt{-1}/2^m)$. Let $\overline{T^{(m)}} = \{W_m^{iR_m(j)}\}_{i,j=0}^{2^m-1}$ so that

$$\overline{F^{(m)}} \{y_i\}_{i=0}^{2^m-1} = \overline{T^{(m)}} \{y_{R(j)}\}_{j=0}^{2^m-1}.$$

For $\{\mathbf{x}_i\}_{i=0}^{2^m-1}$ a lattice in natural order, we have

$$K = \frac{1}{n} \overline{T^{(m) \cdot (-m)}} \overline{T^{(m)}}.$$

Notice that $\overline{T^{(m+1)}} = \left\{ W_{m+1}^{iR_{m+1}(j)} \right\}_{i,j=0}^{2^{m+1}-1}$. For $0 \leq j < 2^m$ we have $R_{m+1}(j) = 2R_m(j)$ so $W_{m+1}^{iR_{m+1}(j)} = W_m^{iR_m(j)}$. For $2^m \leq j < 2^{m+1}$ we have $R_{m+1}(j) = 2R_m(j - 2^m) + 1$ so $W_{m+1}^{iR_{m+1}(j)} = W_m^{iR_m(j-2^m)} W_m^i$. Moreover, for $0 \leq i < 2^m$ we have $W_{m+1}^{2^m+i} = -W_{m+1}^i$. Define $\widetilde{\mathbf{w}}^{(m)} = \{W_{m+1}^i\}_{i=0}^{2^m-1}$. Then

$$\overline{T^{(m+1)}} = \begin{pmatrix} \overline{T^{(m)}} & \text{diag}(\widetilde{\mathbf{w}}^{(m)}) \overline{T^{(m)}} \\ \overline{T^{(m)}} & -\text{diag}(\widetilde{\mathbf{w}}^{(m)}) \overline{T^{(m)}} \end{pmatrix}$$

and $\widetilde{\mathbf{w}}^{(m+1)}$ is the $\alpha = 2$ interlacing of $\widetilde{\mathbf{w}}^{(m)}$ and $W_{m+1} \widetilde{\mathbf{w}}^{(m)}$.

5.2 Digital nets, digitally-shift-invariant kernels, and the FWHT

For $x, y \in [0, 1)$ with $x = \sum_{t=1}^m x_{t-1} b^{-t}$ and $y = \sum_{t=1}^m y_{t-1} b^{-t}$ let

$$x \oplus y = \sum_{t=1}^m ((x_{t-1} + y_{t-1}) \bmod b) b^{-t} \quad \text{and} \quad x \ominus y = \sum_{t=1}^m ((x_{t-1} - y_{t-1}) \bmod b) b^{-t}$$

denote digital addition and subtraction respectively. Note that in base $b = 2$ these operations are both equivalent to the exclusive or (XOR) between bits. For vectors $\mathbf{x}, \mathbf{y} \in [0, 1]^d$, digital operations $\mathbf{x} \oplus \mathbf{y}$ and $\mathbf{x} \ominus \mathbf{y}$ act component-wise. A kernel is said to be digitally-shift-invariant when

$$K(\mathbf{u}, \mathbf{v}) = \widetilde{K}(\mathbf{u} \ominus \mathbf{v})$$

for some \widetilde{K} .

Suppose $n = b^m$ for some $m \in \mathbb{N}_0$ and let $\{\mathbf{x}_i\}_{i=0}^{b^m-1}$ be a digitally shifted digital net in natural order (possibly of higher order and/or with LMS). Following [Jagadeeswaran and Hickernell 2022, Theorem 5.3.1, Theorem 5.3.2], for $b = 2$, the Gram matrix K is nested block Toeplitz which implies the eigendecomposition

$$K = \frac{1}{n} H^{(m)-(m)} H^{(m)}$$

where $H^{(m)}$ is the $2^m \times 2^m$ Hadamard matrix defined by $H^{(0)} = (1)$ and the relationship

$$H^{(m+1)} = \begin{pmatrix} H^{(m)} & H^{(m)} \\ H^{(m)} & -H^{(m)} \end{pmatrix}.$$

Multiplying by $H^{(m)}$ can be done at $O(n \log n)$ cost using the FWHT. Note that K is not necessarily nested block Toeplitz under NUS.

We now describe one dimensional digitally-shift-invariant kernels $K(u, v) = \widetilde{K}(u \ominus v)$ of higher-order smoothness α . Weighted sums over products these one dimensional kernels may be used to construct higher-dimensional kernels e.g. those with product weights

$$K(\mathbf{u}, \mathbf{v}) = \prod_{j=1}^d (1 + \gamma_j (K(u_j, v_j) - 1)).$$

To begin, let us write $k \in \mathbb{N}_0$ as $k = \sum_{\ell=1}^{\#k} k_{a_\ell} b^{a_\ell}$ where $a_1 > \dots > a_{\#k} \geq 0$ are the $\#k$ indices of non-zero digits $k_{a_\ell} \in \{1, \dots, b-1\}$ in the base b expansion of k . Then the k^{th} Walsh coefficient is

$$\text{wal}_k(x) = e^{2\pi\sqrt{-1}/b \sum_{\ell=1}^{\#k} k_{a_\ell} x_{a_\ell+1}}.$$

For $\alpha \in \mathbb{N}$ we also define the weight function

$$\mu_\alpha(k) = \sum_{\ell=1}^{\min\{\alpha, \#k\}} (a_\ell + 1).$$

For $\alpha > 1$, let the digitally-shift-invariant kernel

$$K(x, z) = \sum_{k \in \mathbb{N}_0} \frac{\text{wal}_k(x \ominus z)}{b^{\mu_\alpha(k)}} = \widetilde{K}_\alpha(x \ominus z) \quad (6)$$

have corresponding RKHS \widetilde{H}_α . The following theorem shows \widetilde{H}_α contains smooth functions. The case when $\alpha = 1$ is treated separately in [Dick and Pillichshammer 2005].

THEOREM 5.1. $\widetilde{H}_\alpha \supset H_\alpha$ where H_α is an RKHS with inner product

$$\langle f, g \rangle_{H_\alpha} = \sum_{l=1}^{\alpha-1} \int_0^1 f^{(l)}(x) dx \int_0^1 g^{(l)}(x) dx + \int_0^1 f^{(\alpha)}(x) g^{(\alpha)}(x) dx.$$

PROOF. See appendix A □

The following theorem gives explicit forms of a few higher-order digitally-shift-invariant kernels in base $b = 2$ which are plotted in fig. 3. These kernels are also useful in the computation of the worst-case error of QMC with higher order polynomial-lattice rules as in [Baldeaux et al. 2012]. In fact, their paper details how to compute \tilde{K}_α at $O(\alpha \#x)$ cost where $\#x$ is the number of non-zero digits in the base b expansion of x

THEOREM 5.2. *Fix the base $b = 2$. Let $\beta(x) = -\lfloor \log_2(x) \rfloor$ and $t_\nu(x) = 2^{-\nu\beta(x)}$ where for $x = 0$ we set $\beta(x) = t_\nu(x) = 0$. Then*

$$\begin{aligned}\tilde{K}_2(x) &= -\beta(x)x + \frac{5}{2} [1 - t_1(x)], \\ \tilde{K}_3(x) &= \beta(x)x^2 - 5 [1 - t_1(x)]x + \frac{43}{18} [1 - t_2(x)], \\ \tilde{K}_4(x) &= -\frac{2}{3}\beta(x)x^3 + 5 [1 - t_1(x)]x^2 - \frac{43}{9} [1 - t_2(x)]x \\ &\quad + \frac{701}{294} [1 - t_3(x)] + \beta(x) \left[\frac{1}{48} \sum_{a=0}^{\infty} \frac{\text{wal}_{2^a}(x)}{2^{3a}} - \frac{1}{42} \right].\end{aligned}$$

PROOF. The $\alpha \in \{2, 3\}$ forms are due to [Baldeaux et al. 2012]. The $\alpha = 4$ form is derived in appendix A. \square

5.3 Fast kernel computations and efficient updates

Let us make the general assumptions satisfied by the formulations in the previous two subsections.

- (1) For $n = 2^m$, the Gram matrix $\mathbf{K}^{(m)} \in \mathbb{R}^{n \times n}$ can be written as

$$\mathbf{K}^{(m)} = \mathbf{V}^{(m)\sim(m)} \overline{\mathbf{V}^{(m)}}$$

where $\mathbf{V}^{(m)} \overline{\mathbf{V}^{(m)}} = \mathbf{I}$ and the first column of $\mathbf{V}^{(m)}$, denoted $\mathbf{v}_1^{(m)}$, is the constant $1/\sqrt{n}$

- (2) $\mathbf{V}^{(m)} \in \mathbb{C}^{n \times n}$ satisfies $\mathbf{V}^{(0)} = (\mathbf{1})$ and

$$\mathbf{V}^{(m+1)} = \left(\begin{array}{cc} \mathbf{V}^{(m)} & \mathbf{V}^{(m)} \\ \mathbf{V}^{(m)} \overline{\text{diag}(\tilde{\mathbf{w}}^{(m)})} & -\mathbf{V}^{(m)} \overline{\text{diag}(\tilde{\mathbf{w}}^{(m)})} \end{array} \right) / \sqrt{2}.$$

- (3) $\mathbf{V}^{(m)} \mathbf{y}$ and $\overline{\mathbf{V}^{(m)}}$ are each computable at cost $O(2^m m)$.

For the case of lattice points with shift-invariant kernels and resulting circulant Gram matrices, $\mathbf{V}^{(m)} = \mathbf{T}^{(m)} / \sqrt{2^m}$ is the scaled and permuted Fourier matrix and $\tilde{\mathbf{w}}^{(m)} = \{\exp(-\pi\sqrt{-1}/2^m i)\}_{i=0}^{2^m-1}$, so $\mathbf{V}^{(m)} \mathbf{y}$ and $\overline{\mathbf{V}^{(m)}}$ can be computed using a bit-reversed FFT and bit-reversed IFFT respectively. For the case of digital nets with digitally-shift-invariant kernels and resulting nested block Toeplitz Gram matrices, $\mathbf{V}^{(m)} = \mathbf{H}^{(m)} / \sqrt{n}$ is the scaled Hadamard matrix and $\tilde{\mathbf{w}}^{(m)} = \{1\}_{i=0}^{2^m-1}$, so $\mathbf{V}^{(m)} \mathbf{y}$ and $\overline{\mathbf{V}^{(m)}}$ can be computed using a FWHT and inverse FWHT respectively.

For $\tilde{\mathbf{w}} = \text{diag}(\boldsymbol{\lambda})$, we have

$$\boldsymbol{\lambda} = \sqrt{n}^{-\sim(m)} \overline{\mathbf{v}_1^{(m)}} = \sqrt{n} \overline{\mathbf{V}^{(m)}} \left(\mathbf{V}^{(m)\sim(m)} \mathbf{v}_1^{(m)} \right) = \sqrt{n} \overline{\mathbf{V}^{(m)}} \mathbf{k}_1$$

which can be computed at $O(n \log n)$ cost. Moreover,

$$\mathbf{K} \mathbf{y} = \mathbf{V}^{(m)} (\tilde{\mathbf{y}} \odot \boldsymbol{\lambda}) \quad \text{and} \quad \mathbf{K}^{-1} \mathbf{y} = \mathbf{V}^{(m)} (\tilde{\mathbf{y}} ./ \boldsymbol{\lambda})$$

may each be evaluated at cost $O(n \log n)$ where \odot denotes the Hadamard (component-wise) product and $./$ denotes component-wise division.

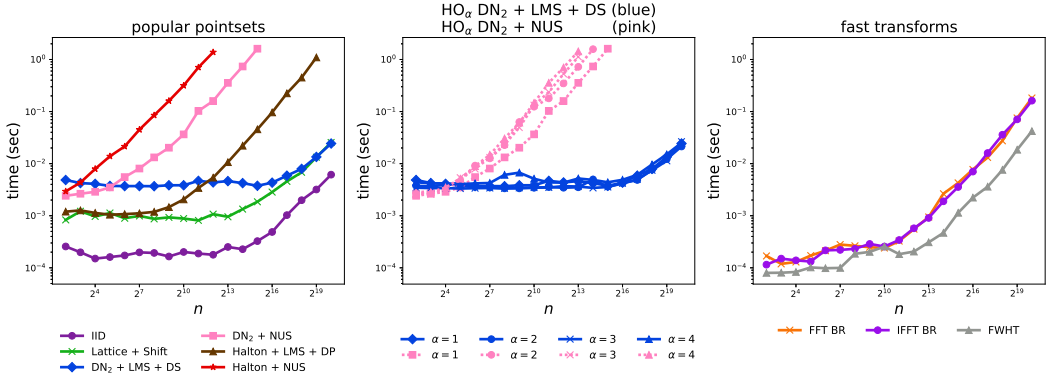


Fig. 5. Comparison of time required to generate IID and low-discrepancy point sets and perform fast transforms. All point sets are generated in a single dimension and with a single randomizations. BR indicates the bit-reversed FFT and IFFT.

To update the solutions of the motivating problems, it is easily shown that

$$\begin{aligned} \mathbf{K}^{(m+1)} \mathbf{y}^{(m+1)} &= \sqrt{2} \begin{pmatrix} \mathbf{V}^{(m)} \left(\tilde{\mathbf{y}}^{(1)} \odot \boldsymbol{\lambda}^{(1)} + \tilde{\mathbf{w}}^{(m)} \odot \tilde{\mathbf{w}}^{(m)} \odot \tilde{\mathbf{y}}^{(2)} \odot \boldsymbol{\lambda}^{(2)} \right) \\ \mathbf{V}^{(m)} \left(\tilde{\mathbf{y}}^{(2)} \odot \boldsymbol{\lambda}^{(1)} + \tilde{\mathbf{y}}^{(1)} \odot \boldsymbol{\lambda}^{(2)} \right) \end{pmatrix} \\ \mathbf{K}^{-(m+1)} \mathbf{y}^{(m+1)} &= \frac{1}{\sqrt{2}} \begin{pmatrix} \mathbf{V}^{(m)} \left(\left(\tilde{\mathbf{y}}^{(1)} \odot \boldsymbol{\lambda}^{(1)} - \tilde{\mathbf{w}}^{(m)} \odot \tilde{\mathbf{w}}^{(m)} \odot \tilde{\mathbf{y}}^{(2)} \odot \boldsymbol{\lambda}^{(2)} \right) ./ \tilde{\mathbf{y}} \right) \\ \mathbf{V}^{(m)} \left(\left(\tilde{\mathbf{y}}^{(2)} \odot \boldsymbol{\lambda}^{(1)} - \tilde{\mathbf{y}}^{(1)} \odot \boldsymbol{\lambda}^{(2)} \right) ./ \tilde{\mathbf{y}} \right) \end{pmatrix} \end{aligned}$$

where $\tilde{\mathbf{y}} = \boldsymbol{\lambda}^{(1)} \odot \boldsymbol{\lambda}^{(1)} - \tilde{\mathbf{w}}^{(m)} \odot \tilde{\mathbf{w}}^{(m)} \odot \boldsymbol{\lambda}^{(2)} \odot \boldsymbol{\lambda}^{(2)}$.

6 Numerical experiments

All numerical experiments were carried out on a 2019 MacBook Pro with an Intel Core i7 processor. Figure 5 compares the wall-clock time required to generate point sets and perform fast transforms. Since scaling in the number dimensions and number of randomizations is linear, point sets are only generated in $d = 1$ with a single randomization. IID points, lattices with shifts, and digital nets with LMS and digital shifts (including higher-order versions) are the fastest sequences to generate. Digital nets in base $b = 2$ exploit Graycode order, integer storage of bit-vectors, and exclusive or (XOR) operations to perform digital addition. Generators of Halton point sets are slower to generate as they cannot exploit these advantages. NUS, especially higher order versions, are significantly slower to generate than LMS randomizations. Even so, higher-order LMS scrambling with digital shifts are sufficient to achieve higher-order RMSE convergence as we shown in the next experiment.

Figure 6 shows higher-order LMS with digital shifts for base $b = 2$ digital nets achieve higher-order RMSE convergence for RQMC methods. Specifically, we are able to achieve an RMSE of $O(n^{-\min\{\alpha, \tilde{\alpha}\} - 1/2 - \delta})$ where α is the higher-order digital interlacing of the net, $\tilde{\alpha}$ is the smoothness of the integrand, and $\delta > 0$ is arbitrarily small. The first two integrands reproduce the experiments of [Dick 2011]. The next two problems are test functions from Derek Bingham's Virtual Library of Simulation Experiments (VLSE)¹⁴. The last two Genz functions are used for forward uncertainty quantification in the Dakota software package [Adams et al. 2020] among other places. For each

¹⁴<https://www.sfu.ca/~ssurjano/uq.html>

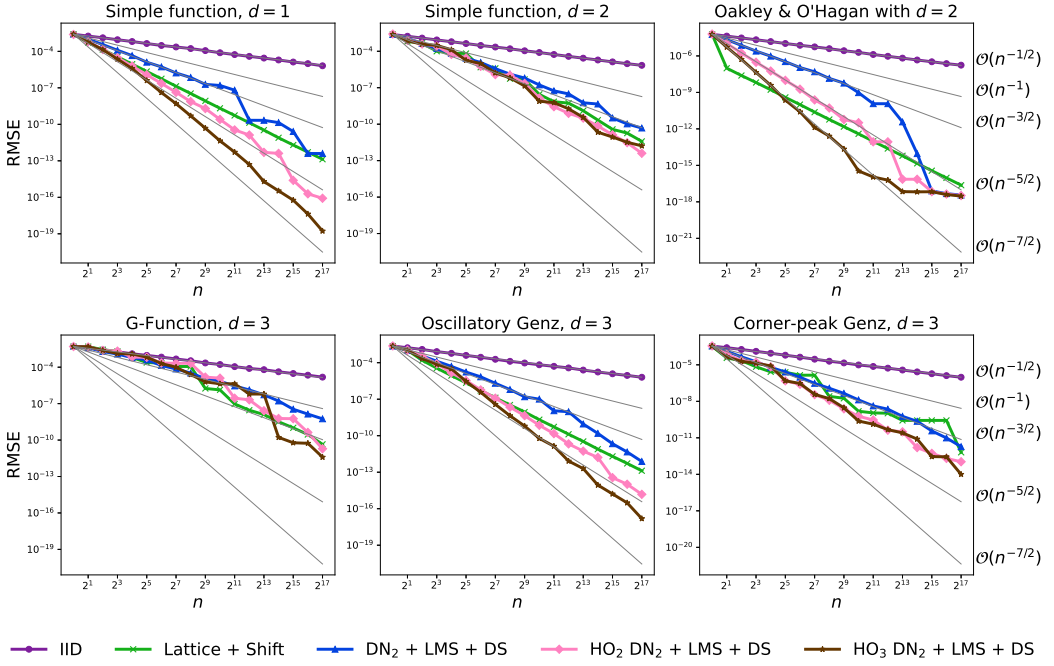


Fig. 6. The RMSE of the RQMC estimate for a few different integrands. Higher-order digital nets with linear matrix scrambling and digital shifts achieve higher-order convergence.

problem, the RMSE of the (Q)MC estimator (1) with $X \sim \mathcal{U}[0, 1]^d$ is approximated using 300 independent randomizations of a LD (or IID) point sets. For lattices, we periodize the integrand using a Baker-transform i.e. we use $\tilde{f}(x) = f(1 - 2|x - 1/2|)$ in place of $f(x)$ in (1). The Baker-transform does not change the expectation. A description of the integrands follows

Simple function, $d = 1$ has $f(X) = Xe^X - 1$. This was used in [Dick 2011] where higher-order digital net scrambling was first proposed.

Simple function, $d = 2$ has $f(X) = X_2 e^{X_1 X_2} / (e - 2) - 1$. This was also used in [Dick 2011].

Oakley & O'Hagan, $d = 2$ has $f(X) = g((X - 1/2)/50)$ for $g(T) = 5 + T_1 + T_2 + 2 \cos(T_1) + 2 \cos(T_2)$, see [Oakley and O'hagan 2002] or the VLSE¹⁴.

G-Function, $d = 3$ has $f(X) = \prod_{j=1}^d \frac{|4X_j - 2| - a_j}{1 + a_j}$ with $a_j = (j - 2)/2$ for $1 \leq j \leq d$, see [Crestaux et al. 2007; Marrel et al. 2009] or the VLSE¹⁴.

Oscillatory Genz, $d = 3$ has $f(X) = \cos\left(-\sum_{j=1}^d c_j X_j\right)$ with coefficients of the third kind $c_j = \exp(k \log(10^{-8})/d)$. This is a common test function for uncertainty quantification which is available in the Dakota software [Adams et al. 2020] among other.

Corner-peak Genz, $d = 3$ has $f(x) = \left(1 + \sum_{j=1}^d c_j X_j\right)^{-(d+1)}$ with coefficients of the second kind $c_j = 1/j^2$. This is also used in the Dakota software [Adams et al. 2020] among others.

7 Conclusion and future work

This work has reviewed routines for generating low-discrepancy point sets, randomizing them, and applying them to fast kernel methods. We have reviewed lattices, digital nets, and Halton point sets

with randomizations spanning shifts, digital permutations, digital shifts, linear matrix scrambling, and nested uniform scrambling. Higher-order scramblings for digital nets were also considered. For kernel methods, we presented classes of kernels which pair with low-discrepancy sequences to accelerate kernel computations. This includes new higher-order digitally shift invariant kernels. The accelerated methods utilize modified fast Fourier transforms and the fast Walsh-Hadamard transform. The presented material has been implemented into the accessible open-source Python library QMCPy.

Acknowledgments

Thank you to Fred J Hickernell, Sou-Cheng T Choi, and Aadit Jain for helpful comments and prototyping. The author would like to acknowledge the support of NSF Grant DMS-2316011.

References

- Brian M Adams, William J Bohnhoff, Keith R Dalbey, Mohamed S Ebeida, John P Eddy, Michael S Eldred, Russell W Hooper, Patricia D Hough, Kenneth T Hu, John D Jakeman, et al. 2020. [Dakota, a multilevel parallel object-oriented framework for design optimization, parameter estimation, uncertainty quantification, and sensitivity analysis: version 6.13 user's manual](#). Technical Report. Sandia National Lab.(SNL-NM), Albuquerque, NM (United States).
- Jan Baldeaux, Josef Dick, Gunther Leobacher, Dirk Nuyens, and Friedrich Pillichshammer. 2012. Efficient calculation of the worst-case error and (fast) component-by-component construction of higher order polynomial lattice rules. [Numerical Algorithms](#) 59, 3 (2012), 403–431.
- P Bratley and B Fox. 2003. Implementing sobols quasirandom sequence generator (algorithm 659). [ACM Trans. Math. Software](#) 29, 1 (2003), 49–57.
- Paul Bratley, Bennett L Fox, and Harald Niederreiter. 1992. Implementation and tests of low-discrepancy sequences. [ACM Transactions on Modeling and Computer Simulation \(TOMACS\)](#) 2, 3 (1992), 195–213.
- Sou-Cheng T Choi, Yuhan Ding, Fred J Hickernell, Jagadeeswaran Rathinavel, and Aleksei G Sorokin. 2022a. Challenges in Developing Great Quasi-Monte Carlo Software. In [International Conference on Monte Carlo and Quasi-Monte Carlo Methods in Scientific Computing](#). Springer, 209–222.
- Sou-Cheng T. Choi, Fred J. Hickernell, Rathinavel Jagadeeswaran, Michael J. McCourt, and Aleksei G. Sorokin. 2022b. Quasi-Monte Carlo Software. In [Monte Carlo and Quasi-Monte Carlo Methods](#), Alexander Keller (Ed.). Springer International Publishing, Cham, 23–47.
- Nicholas Clancy, Yuhan Ding, Caleb Hamilton, Fred J Hickernell, and Yizhi Zhang. 2014. The cost of deterministic, adaptive, automatic algorithms: Cones, not balls. [Journal of Complexity](#) 30, 1 (2014), 21–45.
- Ronald Cools, Frances Kuo, Dirk Nuyens, and Ian Sloan. 2021. Fast component-by-component construction of lattice algorithms for multivariate approximation with POD and SPOD weights. [Math. Comp.](#) 90, 328 (2021), 787–812.
- Ronald Cools, Frances Y Kuo, and Dirk Nuyens. 2006. Constructing embedded lattice rules for multivariate integration. [SIAM Journal on Scientific Computing](#) 28, 6 (2006), 2162–2188.
- Ronald Cools, Frances Y Kuo, Dirk Nuyens, and Ian H Sloan. 2020. Lattice algorithms for multivariate approximation in periodic spaces with general weight parameters. In [75 years of mathematics of computation](#). 93–113.
- T Crestaux, JM Martinez, JMO Le Maitre, and O Lafitte. 2007. Polynomial Chaos Expansion for Uncertainties Quantification and Sensitivity Analysis [PowerPoint Slides]. Retrieved From SAMO 2007. [Retrieved From SAMO 2007 \(2007\)](#).
- Josef Dick. 2008. Walsh spaces containing smooth functions and quasi-Monte Carlo rules of arbitrary high order. [SIAM J. Numer. Anal.](#) 46, 3 (2008), 1519–1553.
- Josef Dick. 2009a. The decay of the Walsh coefficients of smooth functions. [Bulletin of the Australian Mathematical Society](#) 80, 3 (2009), 430–453.
- Josef Dick. 2009b. On quasi-Monte Carlo rules achieving higher order convergence. In [Monte Carlo and Quasi-Monte Carlo Methods 2008](#). Springer, 73–96.
- Josef Dick. 2011. Higher order scrambled digital nets achieve the optimal rate of the root mean square error for smooth integrands. [The Annals of Statistics](#) 39, 3 (2011), 1372 – 1398. <https://doi.org/10.1214/11-AOS880>
- Josef Dick, Peter Kritzer, and Friedrich Pillichshammer. 2022. [Lattice rules](#). Springer.
- Josef Dick, Frances Y Kuo, and Ian H Sloan. 2013. High-dimensional integration: the quasi-Monte Carlo way. [Acta Numerica](#) 22 (2013), 133–288.
- Josef Dick and Friedrich Pillichshammer. 2005. Multivariate integration in weighted Hilbert spaces based on Walsh functions and weighted Sobolev spaces. [Journal of Complexity](#) 21, 2 (2005), 149–195.
- Josef Dick and Friedrich Pillichshammer. 2010. [Digital nets and sequences: discrepancy theory and quasi-Monte Carlo integration](#). Cambridge University Press.

- Henri Faure and Christiane Lemieux. 2009. Generalized Halton sequences in 2008: A comparative study. ACM Transactions on Modeling and Computer Simulation (TOMACS) 19, 4 (2009), 1–31.
- Nathan Jacob Fine. 1949. On the Walsh functions. Trans. Amer. Math. Soc. 65, 3 (1949), 372–414.
- Fino and Algazi. 1976. Unified matrix treatment of the fast Walsh-Hadamard transform. IEEE Trans. Comput. 100, 11 (1976), 1142–1146.
- Bennett L Fox. 1986. Algorithm 647: Implementation and relative efficiency of quasirandom sequence generators. ACM Transactions on Mathematical Software (TOMS) 12, 4 (1986), 362–376.
- Fred Hickernell. 1998. A generalized discrepancy and quadrature error bound. Mathematics of computation 67, 221 (1998), 299–322.
- Fred J Hickernell. 1999. Goodness-of-fit statistics, discrepancies and robust designs. Statistics & probability letters 44, 1 (1999), 73–78.
- Fred J Hickernell, Sou-Cheng T Choi, Lan Jiang, and Lluís Antoni Jiménez Rugama. 2018. Monte Carlo simulation, automatic stopping criteria for. Wiley StatsRef: Statistics Reference Online 1, 1 (2018), 1–7.
- Fred J. Hickernell, Lluís Antoni Jiménez Rugama, and Da Li. 2017. Adaptive Quasi-Monte Carlo Methods for Cubature. arXiv:1702.01491 [math.NA]
- Marius Hofert and Christiane Lemieux. 2023. qrng: (Randomized) Quasi-Random Number Generators. <https://CRAN.R-project.org/package=qrng> R package version 0.0-7.
- Hee Sun Hong and Fred J Hickernell. 2003. Algorithm 823: Implementing scrambled digital sequences. ACM Transactions on Mathematical Software (TOMS) 29, 2 (2003), 95–109.
- The MathWorks Inc. 2022. MATLAB version: 9.13.0 (R2022b). Natick, Massachusetts, United States. <https://www.mathworks.com>
- R. Jagadeeswaran and Fred J. Hickernell. 2019. Fast automatic Bayesian cubature using lattice sampling. Statistics and Computing 29, 6 (Sep 2019), 1215–1229. <https://doi.org/10.1007/s11222-019-09895-9>
- Rathinavel Jagadeeswaran and Fred J Hickernell. 2022. Fast Automatic Bayesian Cubature Using Sobol' Sampling. In Advances in Modeling and Simulation: Festschrift for Pierre L'Ecuyer. Springer, 301–318.
- Stephen Joe and Frances Y Kuo. 2003. Remark on algorithm 659: Implementing Sobol's quasirandom sequence generator. ACM Transactions on Mathematical Software (TOMS) 29, 1 (2003), 49–57.
- Stephen Joe and Frances Y Kuo. 2008. Constructing Sobol sequences with better two-dimensional projections. SIAM Journal on Scientific Computing 30, 5 (2008), 2635–2654.
- Vesa Kaarnioja, Yoshihito Kazashi, Frances Y Kuo, Fabio Nobile, and Ian H Sloan. 2022. Fast approximation by periodic kernel-based lattice-point interpolation with application in uncertainty quantification. Numer. Math. (2022), 1–45.
- Vesa Kaarnioja, Frances Y Kuo, and Ian H Sloan. 2023. Lattice-based kernel approximation and serendipitous weights for parametric PDEs in very high dimensions. arXiv preprint arXiv:2303.17755 (2023).
- Dirk P Kroese, Thomas Taimre, and Zdravko I Botev. 2013. Handbook of monte carlo methods. John Wiley & Sons.
- Frances Y. Kuo and Dirk Nuyens. 2016a. Application of quasi-Monte Carlo methods to elliptic PDEs with random diffusion coefficients - a survey of analysis and implementation. arXiv:1606.06613 [math.NA]
- Frances Y Kuo and Dirk Nuyens. 2016b. Application of quasi-Monte Carlo methods to elliptic PDEs with random diffusion coefficients: a survey of analysis and implementation. Foundations of Computational Mathematics 16 (2016), 1631–1696.
- Frances Y Kuo, Ian H Sloan, and Henryk Woźniakowski. 2004. Lattice rules for multivariate approximation in the worst case setting. In Monte Carlo and Quasi-Monte Carlo Methods 2004. Springer, 289–330.
- Pierre L'Ecuyer, Pierre Marion, Maxime Godin, and Florian Puchhammer. 2021. A Tool for Custom Construction of QMC and RQMC Point Sets. arXiv:2012.10263 [stat.CO]
- Christiane Lemieux. 2009. Monte Carlo and quasi-Monte Carlo sampling. Vol. 20. Springer.
- Pierre L'Ecuyer, Marvin K Nakayama, Art B Owen, and Bruno Tuffin. 2023. Confidence intervals for randomized quasi-Monte Carlo estimators. In 2023 Winter Simulation Conference (WSC). IEEE, 445–456.
- Amandine Marrel, Bertrand Iooss, Beatrice Laurent, and Olivier Roustant. 2009. Calculations of Sobol indices for the Gaussian process metamodel. Reliability Engineering & System Safety 94, 3 (2009), 742–751.
- Jiří Matoušek. 1998. On the L2-Discrepancy for Anchored Boxes. Journal of Complexity 14, 4 (1998), 527–556. <https://doi.org/10.1006/jcom.1998.0489>
- Harald Niederreiter. 1992. Random number generation and quasi-Monte Carlo methods. SIAM.
- Dirk Nuyens and Ronald Cools. 2006. Fast algorithms for component-by-component construction of rank-1 lattice rules in shift-invariant reproducing kernel Hilbert spaces. Math. Comp. 75, 254 (2006), 903–920.
- Jeremy Oakley and Anthony O'hagan. 2002. Bayesian inference for the uncertainty distribution of computer model outputs. Biometrika 89, 4 (2002), 769–784.
- Travis Oliphant. 2006. Guide to NumPy. Vol. 1. Trelgol Publishing USA. <https://ecs.wgtn.ac.nz/foswiki/pub/Support/ManualPagesAndDocumentation/numpybook.pdf>

- Art B Owen. 1995. Randomly permuted (t, m, s) -nets and (t, s) -sequences. In Monte Carlo and Quasi-Monte Carlo Methods in Scientific Computing: Proceedings of a conference at the University of Nevada, Las Vegas, Nevada, USA, June 23–25, 1994. Springer, 299–317.
- Art B Owen. 2003. Variance and discrepancy with alternative scramblings. ACM Transactions of Modeling and Computer Simulation 13, 4 (2003).
- Art B. Owen. 2017. A randomized Halton algorithm in R. arXiv:1706.02808 [stat.CO]
- Art B. Owen. 2018. Monte Carlo theory, methods and examples.
- Art B Owen. 2024. Error estimation for quasi-Monte Carlo. arXiv preprint arXiv:2501.00150 (2024).
- Art B Owen and Zexin Pan. 2024. Gain coefficients for scrambled Halton points. SIAM J. Numer. Anal. 62, 3 (2024), 1021–1038.
- Adam Paszke, Sam Gross, Francisco Massa, Adam Lerer, James Bradbury, Gregory Chanan, Trevor Killeen, Zeming Lin, Natalia Gimelshein, Luca Antiga, et al. 2019. Pytorch: An imperative style, high-performance deep learning library. Advances in neural information processing systems 32 (2019).
- Gottlieb Pirsic. 2002. A software implementation of Niederreiter-Xing sequences. In Monte Carlo and Quasi-Monte Carlo Methods 2000: Proceedings of a Conference held at Hong Kong Baptist University, Hong Kong SAR, China, November 27–December 1, 2000. Springer, 434–445.
- Jagadeeswaran Rathinavel. 2019. Fast automatic Bayesian cubature using matching kernels and designs. Illinois Institute of Technology.
- T Konstantin Rusch, Nathan Kirk, Michael M Bronstein, Christiane Lemieux, and Daniela Rus. 2024. Message-Passing Monte Carlo: Generating low-discrepancy point sets via graph neural networks. Proceedings of the National Academy of Sciences 121, 40 (2024), e2409913121.
- Ian H Sloan and Stephen Joe. 1994. Lattice methods for multiple integration. Oxford University Press.
- Ian H Sloan and Henryk Woźniakowski. 2001. Tractability of multivariate integration for weighted Korobov classes. Journal of Complexity 17, 4 (2001), 697–721.
- S Tezuka. 2002. On randomization of generalized faure sequences. Technical Report. Tech. Rep. RT0494, IBM Tokyo Research Laboratory.
- Xin Tong, Sou-Cheng T Choi, Yuhan Ding, Fred J Hickernell, Lan Jiang, Lluís Antoni Jiménez Rugama, Jagadeeswaran Rathinavel, Kan Zhang, Yizhi Zhang, and Xuan Zhou. 2022. Guaranteed Automatic Integration Library (GAIL): An Open-Source MATLAB Library for Function Approximation, Optimization, and Integration. Journal of Open Research Software 10, 1 (2022).
- Pauli Virtanen, Ralf Gommers, Travis E Oliphant, Matt Haberland, Tyler Reddy, David Cournapeau, Evgeni Burovski, Pearu Peterson, Warren Weckesser, Jonathan Bright, et al. 2020. SciPy 1.0: fundamental algorithms for scientific computing in Python. Nature methods 17, 3 (2020), 261–272.
- Xiaoqun Wang and Fred J Hickernell. 2000. Randomized halton sequences. Mathematical and Computer Modelling 32, 7-8 (2000), 887–899.
- Christopher KI Williams and Carl Edward Rasmussen. 2006. Gaussian processes for machine learning. Vol. 2. MIT press Cambridge, MA.
- Xiaoyan Zeng, Peter Kritzer, and Fred J Hickernell. 2009. Spline methods using integration lattices and digital nets. Constructive Approximation 30 (2009), 529–555.

A Proofs of theorems

For $k \in \mathbb{N}_0$ write

$$\widehat{f}(k) = \int_0^1 f(x) \overline{\text{wal}_k(x)} dx.$$

PROOF OF THEOREM 5.1. Suppose $f \in H_\alpha$. Using the fact that (6) is a Mercer kernel and [Dick 2009a, Theorem 14, Remark 19], we have

$$\|f\|_{\widetilde{H}_\alpha}^2 = \sum_{k \in \mathbb{N}_0} \left| \widehat{f}(k) \right|^2 b^{\mu_\alpha(k)} \leq C_\alpha \sum_{k \in \mathbb{N}} b^{-\mu_\alpha(k)} < \infty$$

for some $C_\alpha < \infty$, so $f \in \widetilde{H}_K$. □

LEMMA A.1 (WALSH COEFFICIENTS OF LOW ORDER MONOMIALS). Fix $b = 2$. Let $f_p(x) := x^p$. When $k \in \mathbb{N}$ write

$$k = 2^{a_1} + \dots + 2^{a_k}$$

where $a_1 > a_2 > \dots > a_{\#k} \geq 0$. Then we have

$$\widehat{f}_1(k) = \begin{cases} 1/2, & k = 0 \\ -2^{-a_1-2}, & k = 2^{a_1} \\ 0, & \text{otherwise} \end{cases},$$

$$\widehat{f}_2(k) = \begin{cases} 1/3, & k = 0 \\ -2^{-a_1-2}, & k = 2^{a_1} \\ 2^{-a_1-a_2-3}, & k = 2^{a_1} + 2^{a_2} \\ 0, & \text{otherwise} \end{cases},$$

$$\widehat{f}_3(k) = \begin{cases} 1/4, & k = 0 \\ -2^{-a_1-2} + 2^{-3a_1-5}, & k = 2^{a_1} \\ 3 \cdot 2^{-a_1-a_2-4}, & k = 2^{a_1} + 2^{a_2} \\ -3 \cdot 2^{-a_1-a_2-a_3-5}, & k = 2^{a_1} + 2^{a_2} + 2^{a_3} \\ 0, & \text{otherwise} \end{cases}.$$

PROOF. The forms for \widehat{f}_1 and \widehat{f}_2 follow from [Dick and Pillichshammer 2010, Example 14.2, Example 14.3]. For $k = 0$ and any $x \in [0, 1)$ we have $\text{wal}_0(x) = 1$, so

$$\widehat{f}_3(x) = \int_0^1 x^3 dx = 1/4.$$

Assume $k \in \mathbb{N}$ going forward. For $k = 2^{a_1} + k'$ with $0 \leq k' < 2^{a_1}$, [Fine 1949, Equation 3.6] implies

$$J_k(x) := \int_0^x \text{wal}_k(t) dt = 2^{-a_1-2} \left[\text{wal}_{k'}(x) - \sum_{r=1}^{\infty} 2^{-r} \text{wal}_{2^{a_1+r}+k}(x) \right].$$

Using integration by parts and the fact that $J_k(0) = J_k(1) = 0$

$$\begin{aligned} \widehat{f}_3(k) &= \int_0^1 x^3 \text{wal}_k(x) dx = \left[x^3 J_k(x) \right]_{x=0}^{x=1} - 3 \int_0^1 x^2 J_k(x) dx \\ &= -3 * 2^{-a_1-2} \left[\widehat{f}_2(k') - \sum_{r=1}^{\infty} 2^{-r} \widehat{f}_2(2^{a_1+r} + k) \right]. \end{aligned}$$

- If $\#k = 1$, i.e. $k = 2^{a_1}$ then

$$\begin{aligned} \widehat{f}_3(k) &= -3 * 2^{-a_1-2} \left[\widehat{f}_2(0) - \sum_{r=1}^{\infty} 2^{-r} \widehat{f}_2(2^{a_1+r} + 2^{a_1}) \right] \\ &= -3 * 2^{-a_1-2} \left[\frac{1}{3} - \sum_{r=1}^{\infty} 2^{-r} 2^{-(a_1+r)-a_1-3} \right] \\ &= 2^{-3a_1-5} - 2^{-a_1-2}. \end{aligned}$$

- If $\#k = 2$ then

$$\widehat{f}_3(k) = -3 * 2^{-a_1-2} \widehat{f}_2(2^{a_2}) = 3 \cdot 2^{-a_1-a_2-4}.$$

- If $\#k = 3$ then

$$\widehat{f}_3(k) = -3 * 2^{-a_1-2} \widehat{f}_2(2^{a_2} + 2^{a_3}) = -3 \cdot 2^{-a_1-a_2-a_3-5}.$$

- If $\#k > 3$ then $\widehat{f}_3(k) = 0$.

□

PROOF OF THEOREM 5.2. Write

$$\tilde{K}_\alpha(x) = 1 + \sum_{1 \leq \nu < \alpha} s_\nu(x) + \tilde{s}_\alpha(x)$$

where s_ν sums over all k with $\#k = \nu$ and \tilde{s}_α sums over all k with $\#k \geq \alpha$. In [Baldeaux et al. 2012, Corollary 1] it was shown that

$$\begin{aligned} s_1(x) &= -2x + 1, \\ s_2(x) &= 2x^2 - 2x + \frac{1}{3}, \\ \tilde{s}_2(x) &= [2 - \beta(x)]x + \frac{1}{2}[1 - 5t_1(x)], \\ \tilde{s}_3(x) &= -[2 - \beta(x)]x^2 - [1 - 5t_1(x)]x + \frac{1}{18}[1 - 43t_2(x)] \end{aligned}$$

from which \tilde{K}_2 and \tilde{K}_3 follow. We now find expressions for s_3 and \tilde{s}_4 from which \tilde{K}_4 follows.

Assume sums over a_i are over \mathbb{N}_0 unless otherwise restricted. Recall from Lemma A.1 that

$$\begin{aligned} x &= \frac{1}{2} - \sum_{a_1} \frac{\text{wal}_{2^{a_1}}(x)}{2^{a_1+2}}, \\ x^2 &= \frac{1}{3} - \sum_{a_1} \frac{\text{wal}_{2^{a_1}}(x)}{2^{a_1+2}} + \sum_{a_1 > a_2} \frac{\text{wal}_{2^{a_1+2a_2}}(x)}{2^{a_1+a_2+3}}, \\ x^3 &= \frac{1}{4} - \sum_{a_1} \frac{\text{wal}_{2^{a_1}}(x)}{2^{a_1+2}} + \frac{3}{2} \sum_{a_1 > a_2} \frac{\text{wal}_{2^{a_1+2a_2}}(x)}{2^{a_1+a_2+3}} - \frac{3}{2} \sum_{a_1 > a_2 > a_3} \frac{\text{wal}_{2^{a_1+2a_2+2a_3}}(x)}{2^{a_1+a_2+a_3+4}} + \sum_{a_1} \frac{\text{wal}_{2^{a_1}}(x)}{2^{3a_1+5}} \end{aligned}$$

so

$$x^3 - \frac{3}{2}x^2 + \frac{1}{2}x = \frac{1}{32} \sum_{a_1} \frac{\text{wal}_{2^{a_1}}(x)}{2^{3a_1}} - \frac{3}{4} \sum_{a_1 > a_2 > a_3} \frac{\text{wal}_{2^{a_1+2a_2+2a_3}}(x)}{2^{a_1+a_2+a_3+3}}$$

and

$$s^{[3]}(x) = \sum_{a_1 > a_2 > a_3} \frac{\text{wal}_{2^{a_1+2a_2+2a_3}}(x)}{2^{a_1+a_2+a_3+3}} = -\frac{4}{3}x^3 + 2x^2 - \frac{2}{3}x + \frac{1}{24} \sum_{a_1} \frac{\text{wal}_{2^{a_1}}(x)}{2^{3a_1}}.$$

Now,

$$\begin{aligned} \tilde{s}_4(x) &= \sum_{\substack{a_1 > a_2 > a_3 > a_4 \\ 0 \leq k < 2^{a_4}}} \frac{\text{wal}_{2^{a_1+2a_2+2a_3+2a_4+k}}(x)}{2^{a_1+a_2+a_3+a_4+4}} \\ &= \sum_{a_1 > a_2 > a_3 > a_4} \frac{\text{wal}_{2^{a_1+2a_2+2a_3+2a_4}}(x)}{2^{a_1+a_2+a_3+a_4+4}} \sum_{0 \leq k < 2^{a_4}} \text{wal}_k(x) \end{aligned}$$

If $x = 0$ then

$$\tilde{s}_4(0) = \sum_{a_1 > a_2 > a_3 > a_4} \frac{1}{2^{a_1+a_2+a_3+4}} = \frac{1}{294}.$$

Going forward, assume $x \in (0, 1)$ so $\beta(x) = -\lceil \log_2(x) \rceil$ is finite. Recall that

$$\sum_{0 \leq k < 2^{a_4}} \text{wal}_k(x) = \begin{cases} 2^{a_4}, & a_4 \leq \beta(x) - 1 \\ 0, & a_4 > \beta(x) - 1 \end{cases}.$$

Moreover, since $\beta(x)$ is the index of the first 1 in the base 2 expansion of x , when $a_4 < \beta(x) - 1$ we have $\text{wal}_{2^{a_4}}(x) = (-1)^{x_{a_4+1}} = 1$ and when $a_4 = \beta(x) - 1$ we have $\text{wal}_{2^{a_4}}(x) = -1$. This implies

$$\begin{aligned} \tilde{s}_4(x) &= \sum_{\substack{a_1 > a_2 > a_3 > a_4 \\ \beta(x)-1 \geq a_4}} \frac{\text{wal}_{2^{a_1+2a_2+2a_3+2a_4}}(x)}{2^{a_1+a_2+a_3+4}} \\ &= \sum_{\substack{a_1 > a_2 > a_3 > a_4 \\ \beta(x)-1 > a_4}} \frac{\text{wal}_{2^{a_1+2a_2+2a_3}}(x)}{2^{a_1+a_2+a_3+4}} - \sum_{a_1 > a_2 > a_3 > \beta(x)-1} \frac{\text{wal}_{2^{a_1+2a_2+2a_3}}(x)}{2^{a_1+a_2+a_3+4}} \\ &=: T_1 - T_2. \end{aligned}$$

The first term is

$$\begin{aligned} T_1 &= \sum_{\beta(x)-1 > a_4} \left(\sum_{a_1 > a_2 > a_3} \frac{\text{wal}_{2^{a_1+2a_2+2a_3}}(x)}{2^{a_1+a_2+a_3+4}} - \sum_{a_4 \geq a_1 > a_2 > a_3} \frac{1}{2^{a_1+a_2+a_3+4}} \right. \\ &\quad \left. - \sum_{a_1 > a_4 \geq a_2 > a_3} \frac{\text{wal}_{2^{a_1}}(x)}{2^{a_1+a_2+a_3+4}} - \sum_{a_1 > a_2 > a_4 \geq a_3} \frac{\text{wal}_{2^{a_1+2a_2}}(x)}{2^{a_1+a_2+a_3+4}} \right) \\ &=: \sum_{\beta(x)-1 > a_4} [V_1(a_4) - V_2(a_4) - V_3(a_4) - V_4(a_4)]. \end{aligned}$$

Clearly $V_1(a_4) = s_3(x)/2$ and V_2 is easily computed. Now

$$\begin{aligned} V_3(a_4) &= \left(\sum_{a_4 \geq a_2 > a_3} \frac{1}{2^{a_2+a_3+3}} \right) \left(\sum_{a_1 > a_4} \frac{\text{wal}_{2^{a_1}}(x)}{2^{a_1+1}} \right) \\ &= \left(\sum_{a_4 \geq a_2 > a_3} \frac{1}{2^{a_2+a_3+3}} \right) \left(s_1(x) - \sum_{a_4 \geq a_1} \frac{1}{2^{a_1+1}} \right) \end{aligned}$$

and

$$\begin{aligned} V_4(a_4) &= \left(\sum_{a_4 \geq a_3} \frac{1}{2^{a_3+2}} \right) \left(\sum_{a_1 > a_2 > a_4} \frac{\text{wal}_{2^{a_1+2a_2}}(x)}{2^{a_1+a_2+2}} \right) \\ &= \left(\sum_{a_4 \geq a_3} \frac{1}{2^{a_3+2}} \right) \left(\sum_{a_1 > a_2} \frac{\text{wal}_{2^{a_1+2a_2}}(x)}{2^{a_1+a_2+2}} - \sum_{a_4 \geq a_1 > a_2} \frac{1}{2^{a_1+a_2+2}} - \sum_{a_1 > a_4 \geq a_2} \frac{\text{wal}_{2^{a_1}}(x)}{2^{a_1+a_2+2}} \right) \\ &= \left(\sum_{a_4 \geq a_3} \frac{1}{2^{a_3+2}} \right) \left(s_2(x) - \sum_{a_4 \geq a_1 > a_2} \frac{1}{2^{a_1+a_2+2}} - \left(s_1(x) - \sum_{a_4 \geq a_1} \frac{1}{2^{a_1+1}} \right) \left(\sum_{a_4 \geq a_2} \frac{1}{2^{a_2+1}} \right) \right). \end{aligned}$$

The second term is

$$\begin{aligned} T_2 &= \sum_{a_1 > a_2 > a_3} \frac{\text{wal}_{2^{a_1+2a_2+2a_3}}(x)}{2^{a_1+a_2+a_3+4}} - \sum_{\beta(x)-1 > a_1 > a_2 > a_3} \frac{1}{2^{a_1+a_2+a_3+4}} + \sum_{\beta(x)-1 > a_2 > a_3} \frac{1}{2^{\beta(x)+a_2+a_3+3}} \\ &\quad - \sum_{a_1 > \beta(x)-1 > a_2 > a_3} \frac{\text{wal}_{2^{a_1}}(x)}{2^{a_1+a_2+a_3+4}} + \sum_{a_1 > \beta(x)-1 > a_3} \frac{\text{wal}_{2^{a_1}}(x)}{2^{a_1+\beta(x)+a_3+3}} \\ &\quad - \sum_{a_1 > a_2 > \beta(x)-1 > a_3} \frac{\text{wal}_{2^{a_1+2a_2}}(x)}{2^{a_1+a_2+a_3+4}} + \sum_{a_1 > a_2 > \beta(x)-1} \frac{\text{wal}_{2^{a_1+2a_2}}(x)}{2^{a_1+a_2+\beta(x)+3}} \\ &=: W_1 - W_2 + W_3 - W_4 + W_5 - W_6 + W_7. \end{aligned}$$

Clearly $W_1 = s_3(x)/2$ and both W_2 and W_3 are easily computed. Similarity in the next two sums gives

$$\begin{aligned} W_5 - W_4 &= \left(\sum_{\beta(x)-1 > a_3} \frac{1}{2^{\beta(x)+a_3+2}} - \sum_{\beta(x)-1 > a_2 > a_3} \frac{1}{2^{a_2+a_3+3}} \right) \left(\sum_{a_1 > \beta(x)-1} \frac{\text{wal}_{2^{a_1}}(x)}{2^{a_1+1}} \right) \\ &= \left(\sum_{\beta(x)-1 > a_3} \frac{1}{2^{\beta(x)+a_3+2}} - \sum_{\beta(x)-1 > a_2 > a_3} \frac{1}{2^{a_2+a_3+3}} \right) \left(s_1(x) - \sum_{\beta(x)-1 > a_1} \frac{1}{2^{a_1+1}} + \frac{1}{2^{\beta(x)}} \right) \end{aligned}$$

Similarity in the final two sums gives

$$W_7 - W_6 = \left(\frac{1}{2^{\beta(x)+1}} - \sum_{\beta(x)-1 > a_3} \frac{1}{2^{a_3+2}} \right) \left(\sum_{a_1 > a_2 > \beta(x)-1} \frac{\text{wal}_{2^{a_1+2a_2}}(x)}{2^{a_1+a_2+2}} \right).$$

where

$$\begin{aligned} \sum_{a_1 > a_2 > \beta(x)-1} \frac{\text{wal}_{2^{a_1+2a_2}}(x)}{2^{a_1+a_2+2}} &= \sum_{a_1 > a_2} \frac{\text{wal}_{2^{a_1+2a_2}}(x)}{2^{a_1+a_2+2}} - \sum_{\beta(x)-1 > a_1 > a_2} \frac{1}{2^{a_1+a_2+2}} + \sum_{\beta(x)-1 > a_2} \frac{1}{2^{\beta(x)+a_2+1}} \\ &\quad - \sum_{a_1 > \beta(x)-1 > a_2} \frac{\text{wal}_{2^{a_1}}(x)}{2^{a_1+a_2+2}} + \sum_{a_1 > \beta(x)-1} \frac{\text{wal}_{2^{a_1}}(x)}{2^{a_1+\beta(x)+1}} \\ &= s_2(x) - \sum_{\beta(x)-1 > a_1 > a_2} \frac{1}{2^{a_1+a_2+2}} + \sum_{\beta(x)-1 > a_2} \frac{1}{2^{\beta(x)+a_2+1}} \\ &\quad + \left(\frac{1}{2^{\beta(x)}} - \sum_{\beta(x)-1 > a_2} \frac{1}{2^{a_2+1}} \right) \left(s_1(x) - \sum_{\beta(x)-1 > a_1} \frac{1}{2^{a_1+1}} + \frac{1}{2^{\beta(x)}} \right). \end{aligned}$$

This implies

$$\begin{aligned} \tilde{s}_4(x) &= \frac{2}{3} (2 - \beta(x)) x^3 + (1 - 5 t_1(x)) x^2 - \frac{1}{9} (1 - 43 t_2(x)) x \\ &\quad - \frac{1}{48} (2 - \beta(x)) \sum_{a_1} \frac{\text{wal}_{2^{a_1}}(x)}{2^{3a_1}} - \frac{1}{294} (7\beta(x) + 701 t_3(x)) + \frac{5}{98} \end{aligned}$$

from which the result follows. \square

Received 20 February 2007; revised 12 March 2009; accepted 5 June 2009

This figure "acm-jdslogo.png" is available in "png" format from:

<http://arxiv.org/ps/2502.14256v1>